

POLITECNICO DI TORINO

Master of Science in Mechatronic Engineering

Master Degree Thesis

Modelling, design and control of a
DC-DC converter for automotive
Thermoelectric-Generator



Tutor

Prof. Marcello Chiaberge

Candidate

Maria Vittoria Morelli

December 2018

Modeling, Design and Control of a DC-DC converter
for Automotive Thermo-electric Generator

ABSTRACT

Nowadays the reuse of wasted energy is an important task for the majority of the fields, particularly for the automotive one. This aims at more efficient systems and reduce pollution, making a product compatible with the requests of active regulations, environment, consumers and producers. With regards to this, in the automotive field, the Exhaust Gas Recirculation (EGR) is becoming an important promise in the energy improvement. The present thesis deals with the modelling, design, control and implementation of a DC-DC power converter to recover energy from the exhaust system in a vehicle.

The strategy is to convert the heat wasted energy into electricity by means of a thermoelectric generator (TEG), which is based on Seebeck effect. The TEG, designed by Magneti Marelli, is connected to a DC-DC converter which allows the recharge of the battery. Many DC-DC converter topologies are examined, few of them are acceptable for the considered application: recharge a battery (nominal voltage 12 V) with an input voltage from 5 V to 55 V and a nominal maximum power of 300 W. In case of extremely high temperature from the exhaust, a flap electro-mechanical valve permits the hot gasses to bypass the TEG in order to avoid damages.

Preliminary losses calculations, complexity, number of components and cost lead to focus on the non-inverting Buck-Boost DC-DC converter topology, in the interest of having both step-up and step-down operation modes.

The thermoelectric generator is modeled and simulated in a model-based environment with the defined DC-DC converter. Maximum Power Point Tracking (MPPT) Perturbation and Observation (P&O) algorithm, for the TEG, is designed and implemented. Dual loop control, for the DC-DC converter, is chosen to control output voltage and current. Design, power dissipation estimations and simulations are validated through prototypes.

Index

ABSTRACT	2
Introduction	5
ENERGY SAVING TECHNOLOGY IN AUTOMOTIVE FIELD	5
AIM AND THESIS LAYOUT	6
Thermoelectric generator	8
SEEBECK EFFECT AND PARAMETERS.....	8
MODELLING AND SIMULATIONS	10
DC-DC Converter	16
DC-DC TOPOLOGIES AND CONSTRAINTS.....	16
NON INVERTING BUCK-BOOST CONVERTER (NIBB).....	18
DESIGN	22
<i>Switching Frequency Selection</i>	22
<i>Inductor Selection</i>	23
<i>Duty Cycle Computations</i>	24
<i>Capacitors Selection</i>	25
<i>Power dissipations and Efficiency</i>	27
Control algorithms and simulations	34
MPPT, ALGORITHMS AND IMPLEMENTATIONS.....	34
<i>Maximum Power Transfer Theorem</i>	34
<i>Perturb and Observe (P&O) algorithm</i>	35
<i>Incremental Conductance (IC) algorithm</i>	36
<i>Modified algorithms and implementation</i>	37
CONTROL DESIGN	43
CONTROL STRATEGIES AND SIMULINK ARCHITECTURES	44
<i>First Control Strategy: Current Loop</i>	45
<i>Second Control Strategy: Dual Loop</i>	47
<i>Third Control Strategy: MPPT + Current Loop</i>	48
Future developments, implementation and conclusions.....	52
FUTURE DEVELOPMENTS.....	52
IMPLEMENTATION	53
CONCLUSION	57
References.....	59

Introduction

ENERGY SAVING TECHNOLOGY IN AUTOMOTIVE FIELD

“Automotive energy recovery systems, such as RBS, turbocharger, and EGR, hold a significant potential to recover the energy wasted while braking or by exhaust gasses during the combustion process. At present, electric vehicles are gaining importance as a substitute to the conventional vehicle powered by IC engine that runs on non-renewable fossil fuels such as petrol and diesel. EGR is the most promising technology which reduces NOx emission by reusing the exhaust gasses reviled during the combustion process.”

As Eshan Hira of Allied Market Research declares, the increase of electrical and hybrid vehicles represents an important reduction of toxic emissions without renouncing the performance of the whole system.

The automotive company Tesla Motors, Inc. in the 2003 was the pioneer of the production of electric vehicles, cars of an improbable future. In the 2018 the company is just one of the several manufacturers: according to “usnews.com”, among the best electric vehicles of the year in U.S. there are cars produced by Tesla and also BMW, Chevrolet, Hyundai, Volkswagen and many more.

Although many advantages are related with the adoption of the electrical motor, lot of constraints are still unresolved such as the battery range or the increasing temperature [1]. Hence another approach in the automotive energy recovery field has been developed: Exhaust Gas Recirculation (EGR) in Internal Combustion (IC) engine vehicles. ICs do not totally convert the chemical energy into mechanical one. In fact, as shown in the Fig.1.1, the greater part of a typical fuel path is wasted in the coolant system and in the exhaust. Only 25% of the energy flows into specific vehicle operations [2].

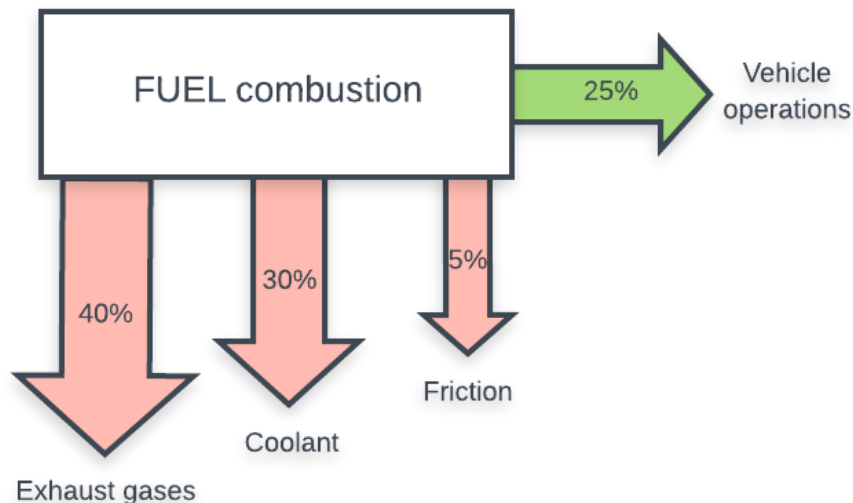


Fig. 1.1 Energy flow path in internal combustion engine

According to “Global Automotive Exhaust Gas Recirculation System Market Size, Share, Trends, Growth and Regional Forecast Industry Report” the EGR system market would grow rapidly up to 2023. The technique is based on the reduction of nitrogen oxide in the environment due to the gasoline and diesel engines of automobiles [3]. In fact, as MAHLE GmbH (Germany) believes, “combustion engine will remain an important drive for a long period of time” [4]. Among the companies which produce EGR systems, there are also

Wells Vehicle Electronics (US), BorgWarner Inc (US), Cambustion Ltd (UK), Delphi ANSYS Inc (UK), Denso Corporation (Japan), and many more.

For a better understanding and for supporting market analysis, the EGR system market could be organized in different segmentations:

- Product type: EGR valve (Fig. 1.2a), EGR Cooler (Fig. 1.2b), EGR pipe (Fig. 1.2c);

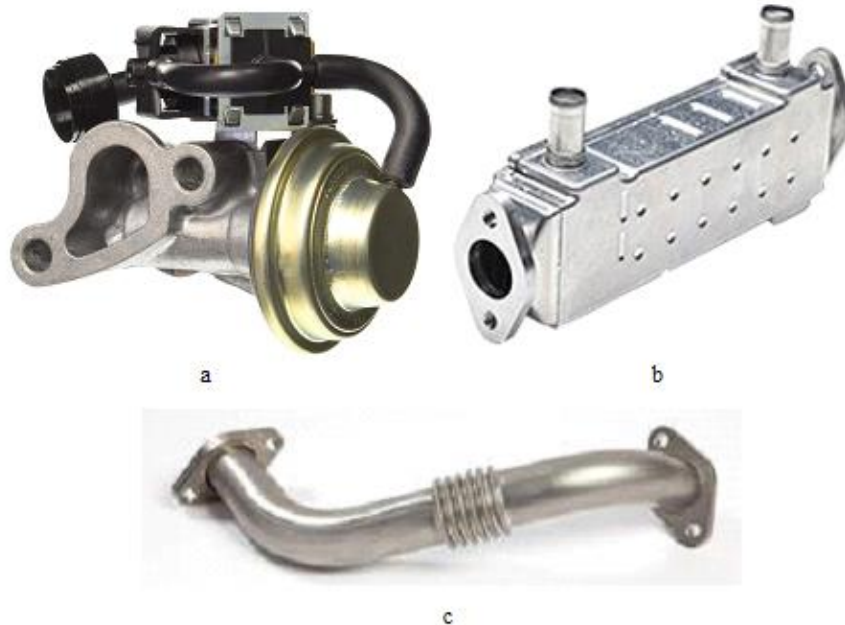


Fig. 1.2 EGR system components

- Vehicle Type: Passenger vehicle, light commercial vehicle, heavy and commercial vehicle;
- Application: Gasoline, Diesel;
- Regions: North America, Europe, Asia, Rest of the world.

Geographically, the market, in the last two years, raised especially in China and Japan. The reason lies in the fact that those countries did not suffer from the global economic crisis of 2008-2009. Instead they demonstrated a continuous development, particularly in the automotive field, which led to great sales and more improvements.

AIM AND THESIS LAYOUT

The exhaust heat recovering is a potential solution in saving fuel and reducing dangerous emissions, with low costs and remarkable efficiency improving. The thermoelectric conversion, based on the Seebeck effect, represents the beginning of this energy recovering project.

The present work consists in developing a device by means of the usage of a TEG, which is placed on the exhaust, to recharge the battery of a vehicle. The maximum power has to be transferred from the TEG to the load through a DC-DC converter, which aims at regulating parameters into a specific range (nominal voltage of the battery 12 V).

The usage of Maximum Power Point Tracking algorithms allow reaching the best working point, in order to get the best performance of the system.

Hence the objective of the thesis could be explained as well by Fig. 1.3:

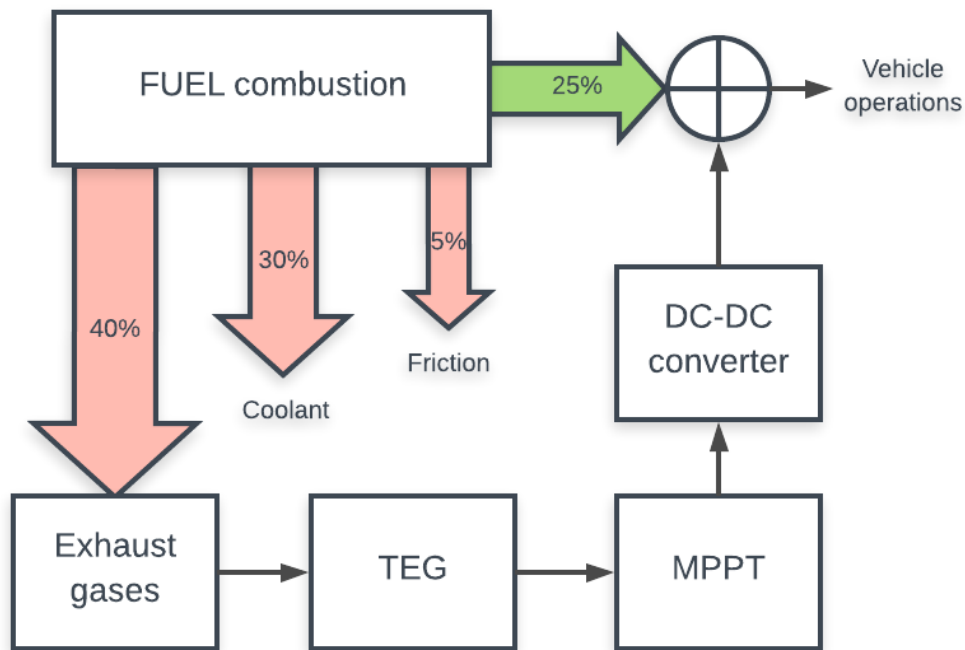


Fig. 1.3 Thesis objective scheme

Prototypes are realized and tested allowing the observation of the correctness of the design and the power dissipations and efficiency calculations.

Moreover in the final project a bypass flap actuator would be connect to the device and implemented in the vehicle in order to shut off quickly dangerous hot gasses from the exhaust, because the purpose is to guarantee the life and reliability of the entire energy recovery system in all situations.

The layout of the thesis is planned in chapters to describe separately the different elements of the entire project. In fact second chapter illustrates the functioning of the TEG, the third the DC-DC converter. Then the control and the simulation parts are explained in details, defining initially the MPPT and its various algorithms and implementations. Conclusions are made with some mentions about future developments.

Thermoelectric generator

SEEBECK EFFECT AND PARAMETERS

Thomas Johann Seebeck discovered in 1822 that two electrical conductors or semiconductors produce a voltage difference in the presence of a temperature gradient. Therefore, the Seebeck effect is the phenomenon consisting in the conversion of a temperature difference into electrical energy. This behavior is widely used with thermocouples for the temperature measurements and generally with thermoelectric generators.

The simplest TEG module is made of a couple of N-type and P-type materials connected at their end. As shown in the figure below (Fig.2.1), the semiconductors are placed electrically in series and thermally in parallel. When the gradient of temperature ΔT is high enough, the electrons flow from the hot to the cold side of the materials, generating an electromotive force. Hence, if a circuit is attached, a direct current is generated [5].

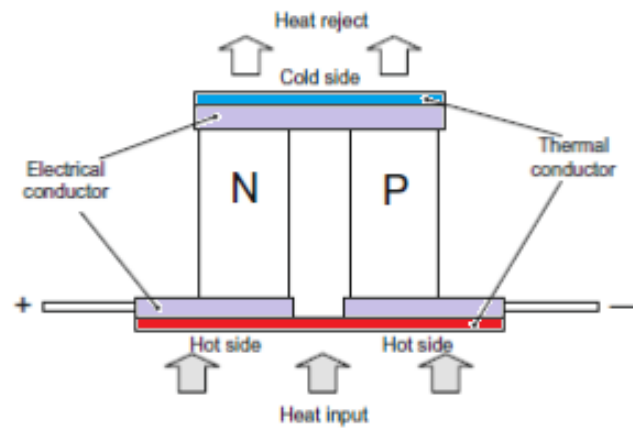


Fig. 2.1 Thermoelectric module - Seebeck effect

The electromotive force e_{TEG} produced is directly proportional to the temperature difference $T_{hot} - T_{cold}$ and it is specified by the Seebeck coefficient α , unique for each material used[6]:

$$e_{TEG} = \alpha \Delta T = \alpha (T_{hot} - T_{cold}) \quad (1)$$

As validated from the equation (1), there is a linear correlation between the voltage produced and the Seebeck coefficient α . Therefore, to guarantee an appropriate performance of the thermoelectric (TE) material, a significant Seebeck coefficient value is needed. If it is low the voltage across the conductors could be not large enough. Each grade of temperature can produce only few millivolts. To increase the output voltage, a possible solution consists in positioning many TE devices in series. Moreover, if the output current has to be risen, the TE modules have to be placed in parallel (Fig. 2.2).

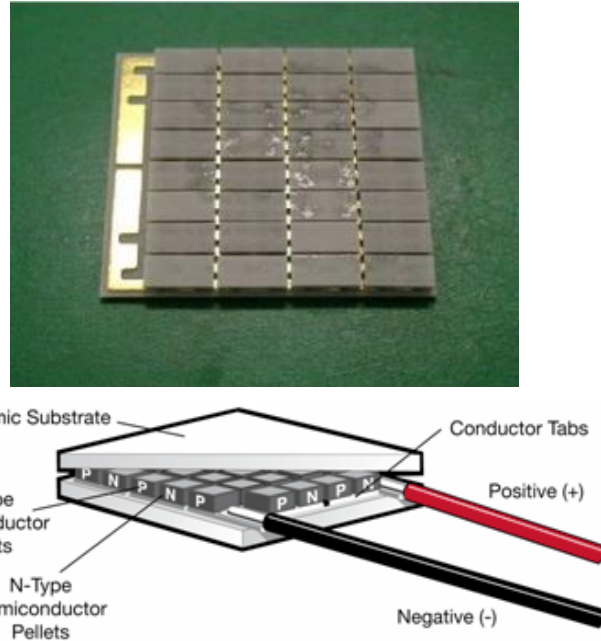


Fig. 2.2 TEG architecture

Other parameters need to be considered. In fact, the efficiency of a TE material depends mainly on the figure of merit ZT , based on Seebeck coefficient α , heat conductivity λ and electrical resistivity ρ :

$$ZT = \frac{\alpha^2 T}{\rho \lambda} \quad (2)$$

Combinations of high Seebeck coefficient, low conductivity and low electrical resistivity permits an adequate value of the figure of merit, the main characterization of TE modules. ZT , as depicted in the equation (3) below, assesses the efficiency and the quality of the conversion of the heat into electricity.

$$\eta = \frac{\Delta T}{T_{hot}} \left(\frac{\sqrt{1 + ZT} - 1}{\sqrt{1 + ZT} + T_{cold}/T_{hot}} \right) \quad (3)$$

An important aspect to consider is also the material used to shape the TE modules. There are several TEG created for several project, thus using very different materials each offering advantages, in terms of efficiency or cost. An improvement could be making the device flexible. Examples are polydimethylsiloxane (PDMS) based TEGs or SU-8 based TEGs [7]. Instead among more conventional TEG, materials commonly employed are Bismuth Telluride (Bi_2Te_3) and Lead Telluride (PbTe), which are characterized by figure of merit $ZT = 1$. Nowadays the market is becoming more and more challenging and finding new materials which can have higher figure of merit is the purpose. The research is focused on the increasing of the Seebeck coefficient or reducing the thermal conductivity. In order to achieve those goals it is common to study the nanostructure of the materials.

MODELLING AND SIMULATIONS

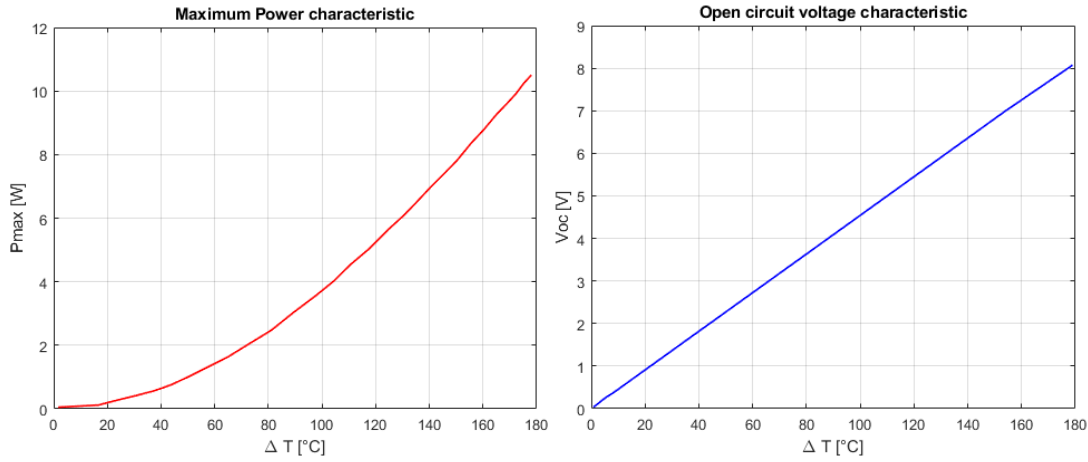


Fig. 2.3 TEG Underfloor cell characteristic

The characteristic of the single cell which contains a TE module is shown above in Fig. 2.3. The maximum power and the open circuit voltage are represented as a function of the delta temperature ΔT . The values are extracted from the datasheet, given by Magneti Marelli, and imported in Matlab (first graph Fig. 2.4). Because of the Seebeck effect, it is simple to notice that the higher the gradient of temperature, the higher the output voltage V_{oc} across the TE modules.

From the elaboration of these data, the coefficients of the voltage ramp, function of the temperature, are computed:

$$V_{OC} = m_v \cdot \Delta T + q_v \quad (4)$$

With

$$q_v = -0.039636 \quad m_v = 0.045785$$

From the reconstruction of V_{oc} , it is obtained the relation between current and voltage at different temperature gradients (second graph Fig. 2.4). The star points stand for the maximum power at each temperature. The third graph of Fig. 2.4 represents the equivalent resistance characteristic and its linearization. The coefficients are calculated and expressed below:

$$R_{eq} = m_r \cdot \Delta T + q_r \quad (5)$$

With

$$q_r = 1.2111 \quad m_r = 0.0018764$$

Therefore the obtained electrical model of a single cell is defined by equations (4) and (5), that is a voltage source with an internal resistance.

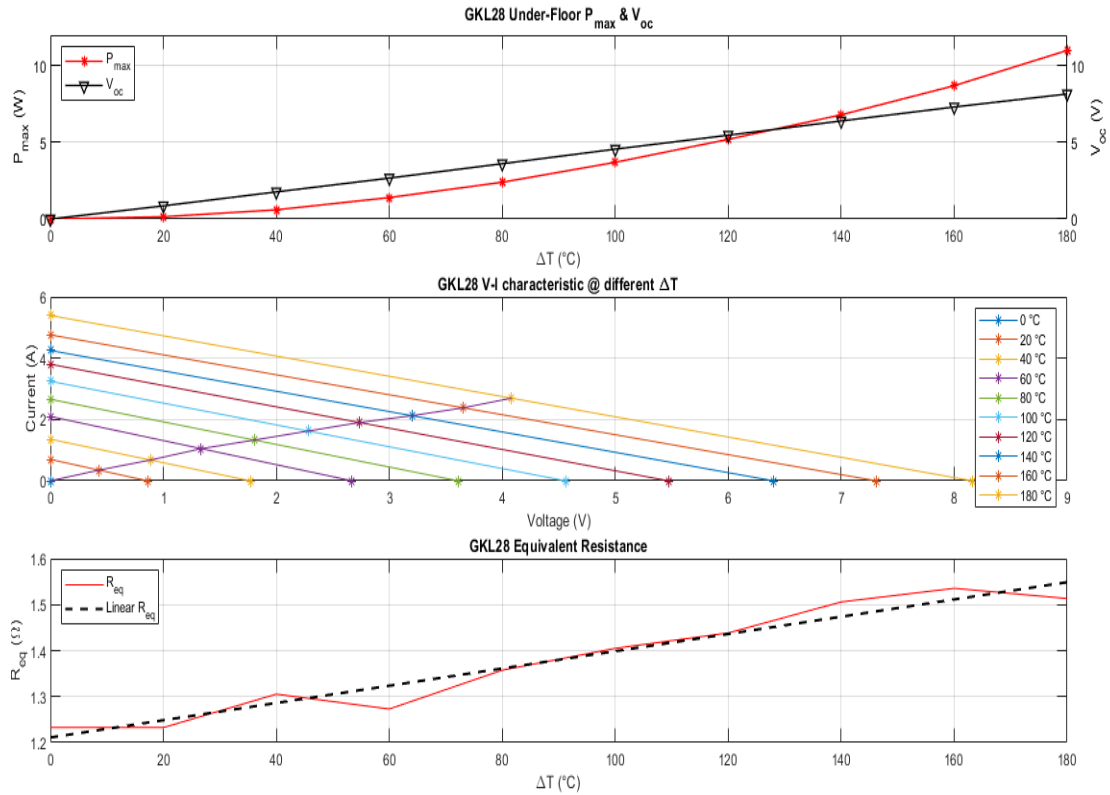


Fig. 2.4 TEG characteristic single cell on Matlab

The objective is to transfer the maximum power from the thermoelectric generator to the load. Hence the output voltage and current of the TEG should be the values corresponding to the star points in the second graph, which are exactly the half of their maximum values (6):

$$V_{mp} = \frac{V_{OC}}{2} \quad (6)$$

$$I_{mp} = \frac{P_{MAX}}{V_{mp}} \quad (7)$$

V_{mp} and I_{mp} will be then the inputs of the DC-DC converter described in next chapters.

The results of a single cell would not be enough for an adequate performance of the entire system. In fact the thermoelectric generator used in the present work, is a combination of 24 cells connected in series and parallel; in order to have a total output voltage less than 60 V the final configuration is 6 in series and 4 in parallel (Fig. 2.5):

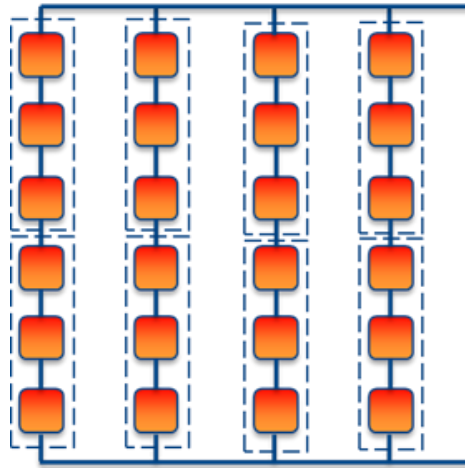


Fig. 2.5 TEG structure used

Different data are then examined and imported in Matlab. In Fig. 2.6 three different graphs are shown:

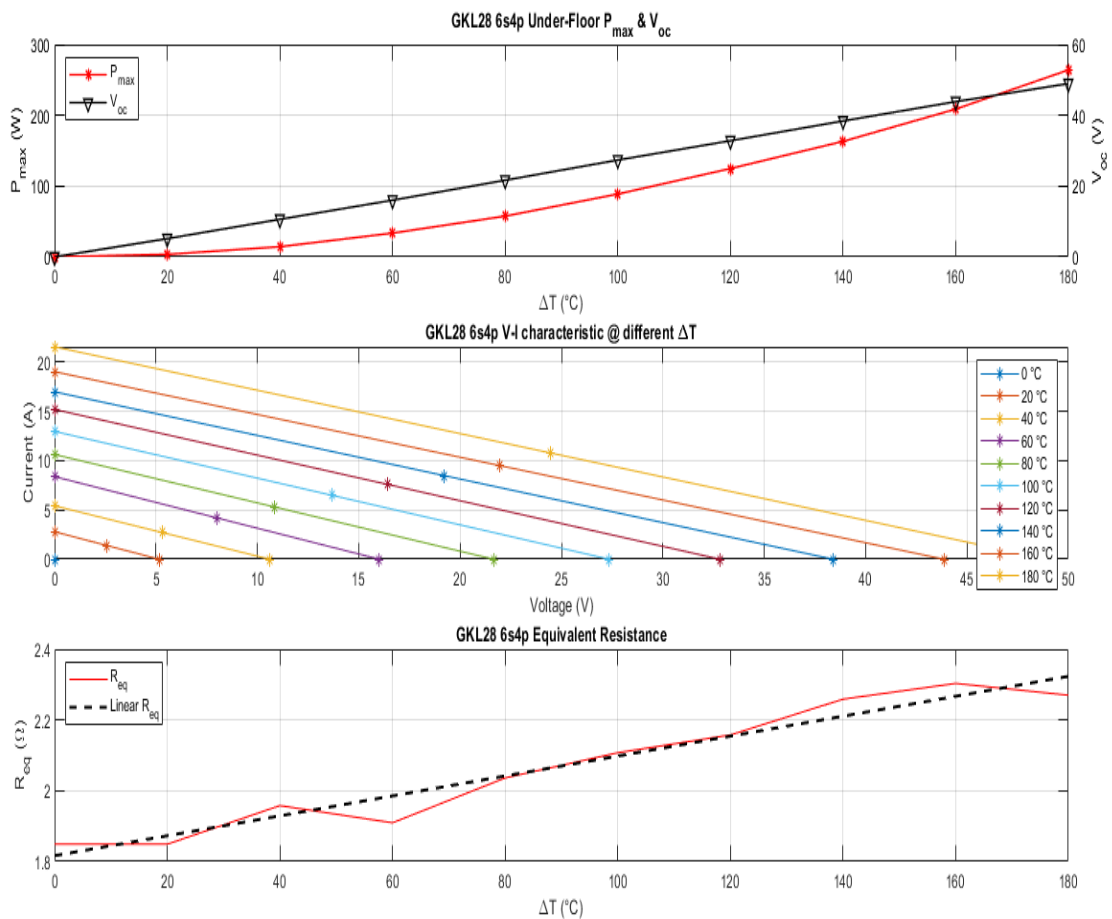


Fig. 2.6 TEG characteristic 24 cells on Matlab

The results change because of the addition of the new cells. Take in to account that:

$$n_s = \text{number of cells in series}$$

$$n_p = \text{number of cells in parallel}$$

The obtained values are upgraded in this way:

$$V_{OCtot} = V_{OC} * ns \quad (8)$$

$$P_{MAXtot} = P_{MAX} * ns * np \quad (9)$$

With:

$$q_{vtot} = -0.23782$$

$$m_{vtot} = 0.27471$$

$$q_{rtot} = 1.8166$$

$$m_{rtot} = 0.0028146$$

And moreover:

$$V_{mp} = \frac{V_{OCtot}}{2} \quad (10)$$

$$I_{mp} = \frac{P_{MAXtot}}{V_{mp}} \quad (11)$$

In next chapters with the annotation V_{mp} and I_{mp} it is considered the output voltage and current from the TEG with 24 cells.

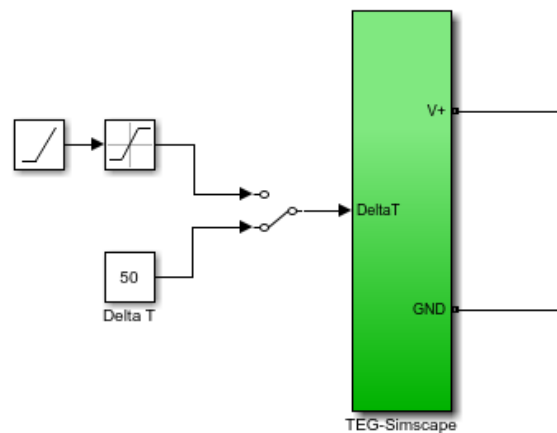


Fig. 2.7 Simulink TEG model, outside

In the Simulink environment the input of the TEG is represented by the ΔT , that is the temperature difference between the hot and the cold side of the all TE modules. The behavior is simulated with a constant value or with a slow ramp. Inside the green block (Fig. 2.7) the TEG is then modeled in a circuit as depicted below (Fig. 2.8):

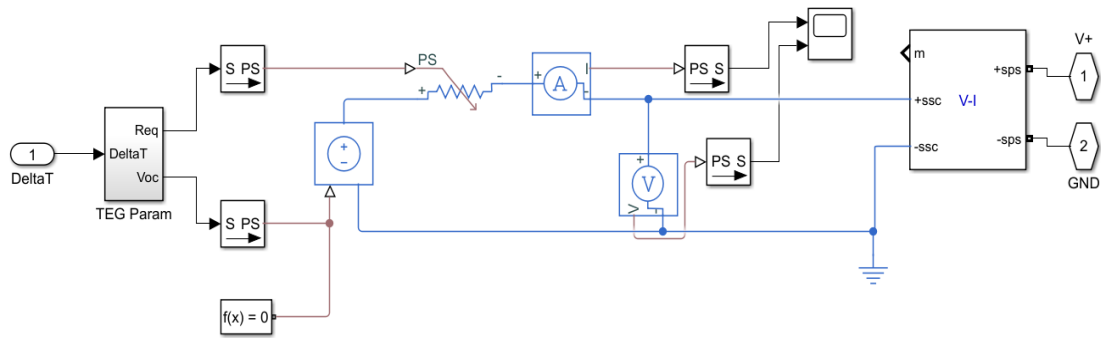


Fig. 2.8 Simulink TEG model, inside

The parameters calculated in the workspace are transferred to the voltage generator and to the variable resistance.

To evaluate the correctness of the model, a controlled current source, supplied with a current ramp, is applied at the output of the TEG, to simulate a load (Fig. 2.9):

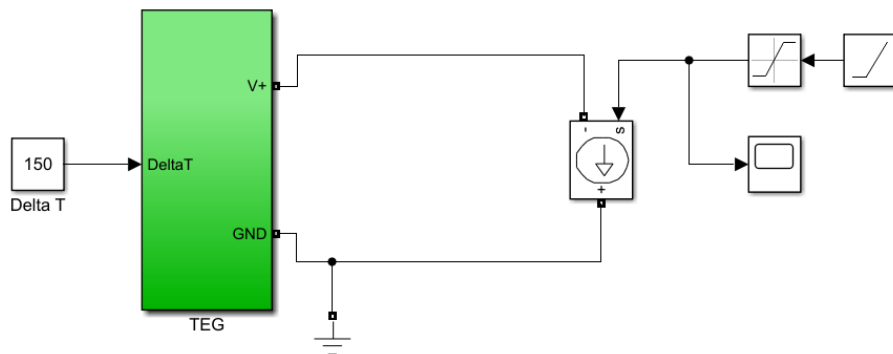


Fig. 2.9 TEG with controllable current source

The performance of the TEG seems to behave as the supposed one. As in Fig 2.10, current and voltage have the opposite orientation and the maximum power is obtained at the half of their maximum values. In this case, with $\Delta T = 150^\circ\text{C}$, $P_{\text{max}} = 189 \text{ W}$; $V_{\text{mp}} = 20.6 \text{ V}$; $I_{\text{mp}} = 9.2 \text{ A}$.

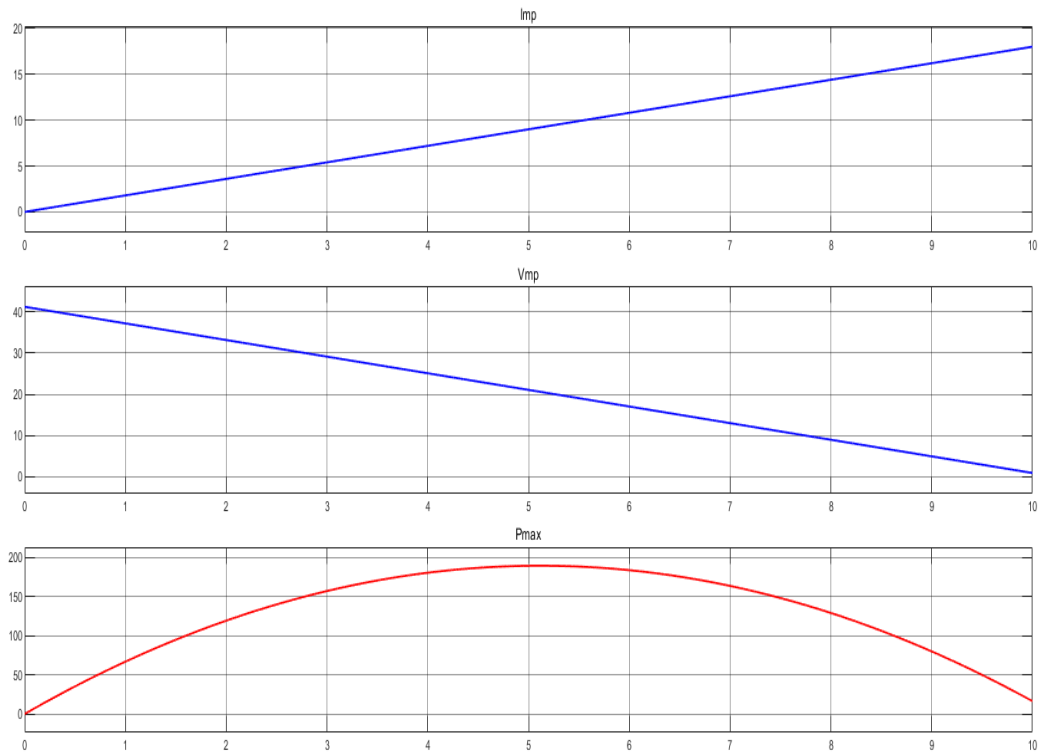


Fig. 2.10 Simulink TEG simulation

DC-DC Converter

DC-DC TOPOLOGIES AND CONSTRAINTS

The present thesis deals with the realization of a DC-DC converter to take advantage of the voltage across the output of the TEG. DC-DC converters can regulate an unregulated input voltage for a specific load [8] (Fig. 3.1).



Fig. 3.1 DC-DC converter regulation scheme

The usage of this topology of converters, DC-DC switch-mode power converters, leads to some **advantages** [9]:

- Efficiency is generally high, from 70% to 95%;
- They can be designed with very small components: on one hand high efficiency requires less coolers, on the other hand high frequencies permits the usage of reduced components. These converters are usually 80% lighter with respect to the analogous linear supplies [10];
- Smaller components correspond to smaller packaging and then lower costs;
- They could have multiple outputs which could be higher or lower values with respect to the input and also with different polarity.

Drawbacks are also presented:

- DC-DCs are complex to design and especially to control;
- They produce high electromagnetic noise;
- They are slow systems: with a reduced bandwidth if the load changes, the output voltage changes slower.

The device to be realized has to be light, easy to implement on a car, cheap and functional. DC-DC converters are adequate for this purpose, and the various limitations presented above could be considered negligible compared to the amount of advantages regarding this choice.

Below in the Table 1 there is a list of the main DC-DC converters which could be considered to be connected to the output of the TEG. The table shows the electrical circuit of each topology, the operation mode

(V_i = input voltage; V_o = output voltage) and the TEG eligibility. Green point approves the converter for the present task; yellow point does not mean to be the optimal solution; red point considers the converter not suitable.

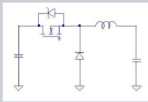
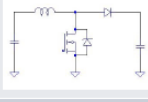
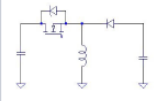
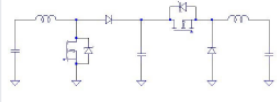
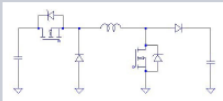
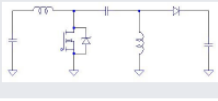
Topology	Schematics	Operation	TEG eligibility
Buck		$V_o < V_i$	It works only for $\Delta T > 240^\circ\text{C}$ Moreover for low ΔT 's energy flows from the battery to the TEG ●
Boost		$V_o > V_i$	It works only for $\Delta T < 150^\circ\text{C}$ For higher ΔT 's energy is delivered to the battery in an uncontrolled way ●
Buck-Boost (Polarity-Inverting)		$ V_o > V_i $ $V_o < 0$	TEG is series connected to the battery resulting in possible voltage $> 60\text{V}$  ●
Boost and Buck cascaded		$V_o > < V_i$ $V_o > 0$	Input and output voltage ranges compatible with the operation of TEG in a vehicle. Dual stage. ●
Buck-Boost (non Polarity-Inverting)		$V_o > < V_i$ $V_o > 0$	Input and output voltage ranges compatible with the operation of TEG in a vehicle. Two working modes: <ul style="list-style-type: none"> • Buck-Boost • Buck or Boost or Buck-Boost ●
SEPIC		$V_o > < V_i$ $V_o > 0$	Input and output voltage ranges compatible with the operation of TEG in a vehicle. ●

Table 1

Buck converter is a basic topology which permits to step down the input voltage to a specific output voltage reference. **Boost** converter, instead, is a step-up converter: it increases the voltage input to a higher value. **Buck-Boost** converter represents the perfect combination of the above converters, allowing the working mode in every situation. Therefore, only three of the aforementioned topologies in the table are acceptable for the application: Boost and Buck cascaded, Non Inverting Buck-Boost (NIBB) and SEPIC. Considering preliminary losses calculation, complexity, number of components and cost, the development is focused on the non-inverting buck-boost topology.

NON INVERTING BUCK-BOOST CONVERTER (NIBB)

The electrical circuit depicted in the Fig. 3.2 represents the basic topology from which the modelling started.

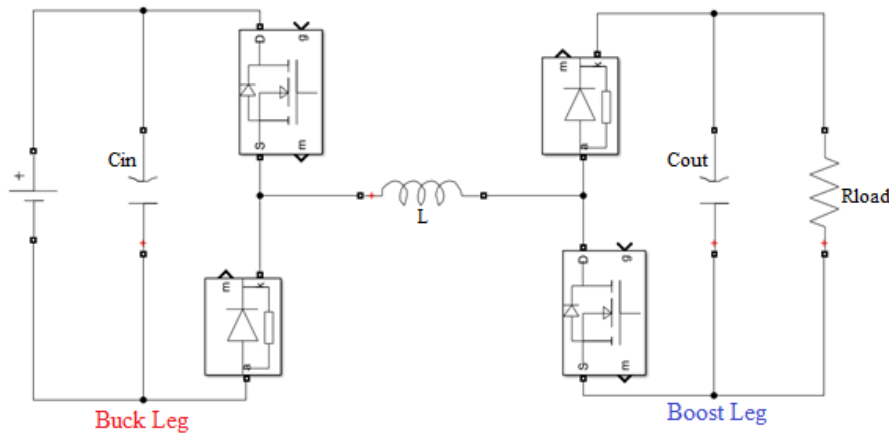


Fig. 3.2 Non inverting Buck-Boost converter electrical circuit

This is a **two-switch non inverting Buck-Boost converter**, modeled with two switches, a single inductor, input and output capacitors and two diodes. Then the converter is characterized by diode (or nonsynchronous) rectification.

Two different parts are distinguishable: the first stage is the Buck leg, consisting of switch SW1 and diode D1; while the second stage is defined Boost leg, made of switch SW2 and diode D2. The voltage source represents the input of the DC-DC and thus the output of the TEG. The load, now is considered as a simple resistor; next it will be replaced by a battery.

Considering the Buck leg, when SW1 is closed (Fig.3.3), hence when it is ON, the current flow and passed through the inductor L also because the diode D1 stop it (it is in OFF mode).

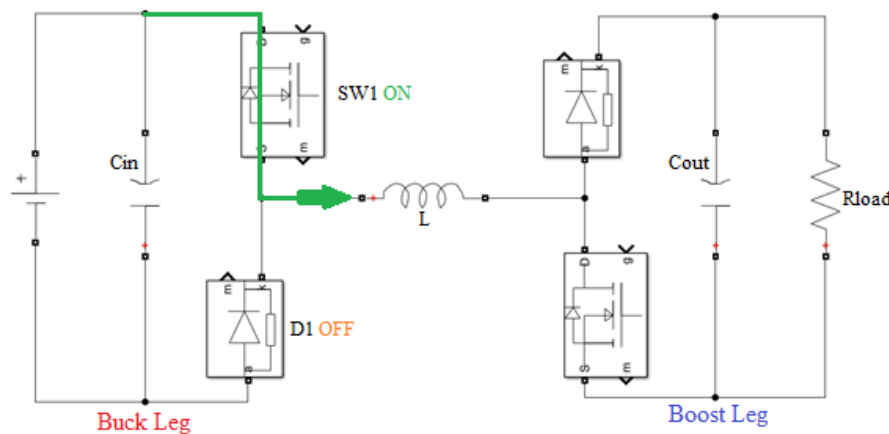


Fig. 3.3 NIBB circuit SW1 on; D1 off

When SW1 is OFF, diode D1 is ON and it permits the flowing of the current from the down branch to the inductor (Fig.3.4):

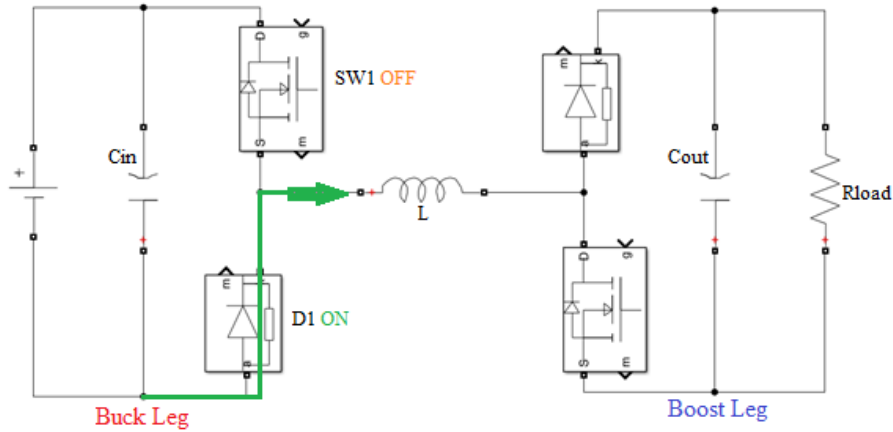


Fig. 3.4 NIBB circuit SW1 off; D1 on

The pictures above illustrated the full Buck operation mode of the circuit. Main parameters are summarize in Table 2:

Operation Mode	Input Voltage	SW1	D1	d1
Full Buck	$V_{in} < (V_{out} - p)$	ON	OFF	100 %
		OFF	ON	0 %

Table 2

Same reasoning could be applied to the Boost leg: when SW2 is ON, D2 is OFF (Fig. 3.5)

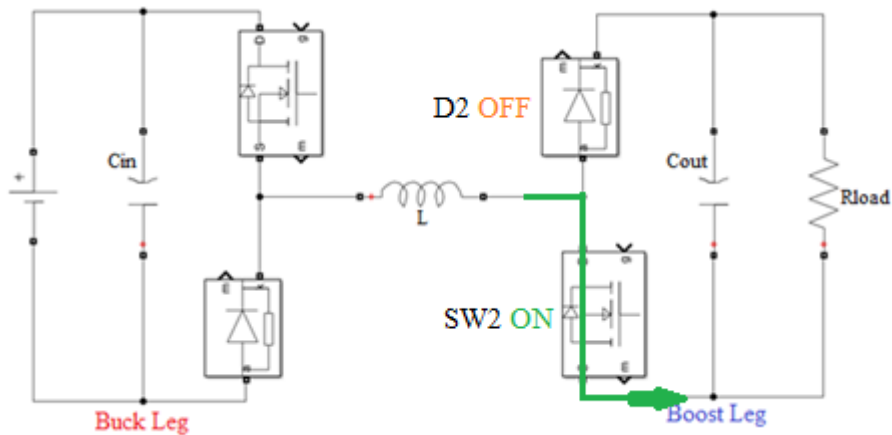


Fig. 3.5 NIBB circuit SW2 on; D2 off

and when SW2 is OFF the D2 is considered in ON mode (Fig. 3.6).

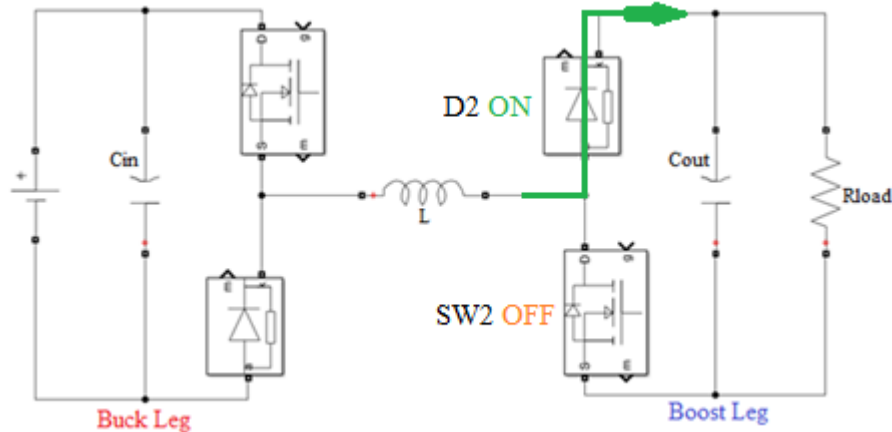


Fig. 3.6 NIBB circuit SW2 off; D2 on

In Table 3 full Boost operation mode is defined:

Operation Mode	Input Voltage	SW2	D2	d2
Full Boost	$V_{in} > (V_{out} + p)$	ON	OFF	100 %
		OFF	ON	0 %

Table 3

Consequently, the important aspect of this circuit topology is the synchronization of the switches (so the duty cycle) because their opening and closing can cause different working operations. Taking into consideration the value of the input voltage, the Buck-Boost operation mode in this circuit topology is possible when (Table4):

Operation Mode	Input Voltage	SW1	D1	d1
		SW2	D2	d2
Buck-Boost	$(V_{out} - p) < V_{in} < (V_{out} + p)$	switching	ON and OFF	variable

Table 4

The peculiar condition of the Buck-Boost mode is based on the switching of both SW1 and SW2, hence on a variable (= var in Table 4) duty cycle. Then also diodes turn ON and OFF very fast.

It is necessary to remember that the input voltage depends on the maximum power of the TEG ($V_{in} = V_{mp}$), hence on the temperature gradient. Different temperatures means different operation modes. In our case the load to be charged is a battery of 13.5 V ($V_{out} = V_{batt}$). From the dataset given by Magneti Marelli, when V_{mp} is approximately close to 13.5V the delta temperature is around 100°C. Buck-Boost region is defined with the parameter p , then a little up and a little down the voltage of the battery.

With $p = 2$, the distinction of the three regions are shown in the table (Table 5) and figure below (Fig. 3.7):

Working Mode	Input Voltage [V]	Input Temperature [°C]
Boost	$V_{mp} < 11.5$	$\Delta T < 85$
Buck	$V_{mp} > 15.5$	$\Delta T > 113$
Buck-Boost	$11.5 < V_{mp} < 15.5$	$84 < \Delta T < 114$

Table 5

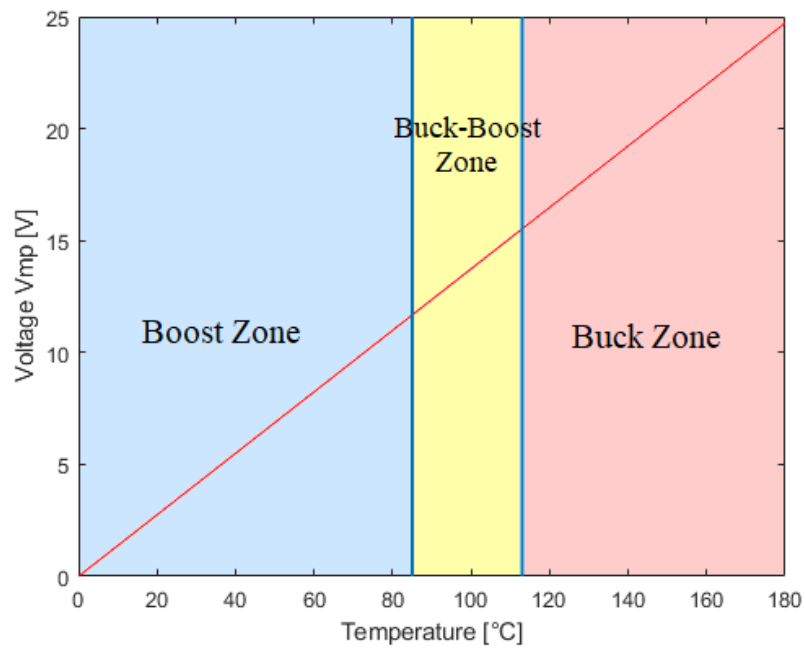


Fig. 3.7 Operation mode Zones

DESIGN

Switching Frequency Selection

The first task in designing a DC-DC converter is to set the switching frequency f_{sw} . The value of f_{sw} takes into account the power level of the system and the specifications of all the components. This choice involves the management of reaching some compromises. In fact the higher is the frequency the smaller are the filter components and faster is the response of the system [11]. On the other hand, at high frequencies the power dissipations of the switches become no more negligible and the correct behavior of the system could not be guaranteed. Moreover the inductor would be larger and heavier.

DC-DC converters are generally characterized by two operating mode, according to the current which flows through the inductor:

- Continuous Conduction Mode (CCM): the inductor current i_L fluctuates but never reaches zero; (Fig. 3.8 represents a general inductor current in a Buck converter in CCM)

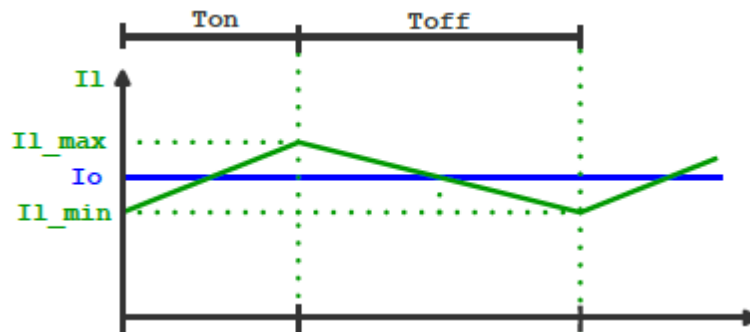


Fig. 3.8 Inductor current Buck converter CCM

- Discontinuous Conduction Mode (DCM): there is an interval in which i_L is equal to zero. (Fig. 3.9 represents a general inductor current in a Buck converter in DCM)

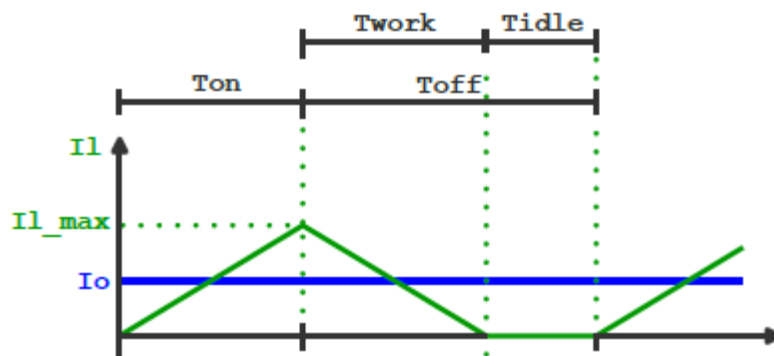


Fig. 3.9 Inductor current Buck converter DCM

Inductor Selection

The selection of the inductor should be based on various factors [12]:

- Peak-to-peak inductor ripple current (*ripple*), which is set at 0.3;
- RMS currents;
- Saturation current;
- Size, weight and cost.

The equations to choose the inductor are:

$$L_{Buck} = \frac{V_{batt}(V_{mp} - V_{batt})}{ripple * I_{out}V_{mp}f_{sw}} \quad (12)$$

$$L_{Boost} = \frac{V_{mp}^2(V_{batt} - V_{mp})}{ripple * I_{out}V_{batt}^2f_{sw}} \quad (13)$$

In the Buck-Boost region the value of the inductance is maintained constant.

Fig. 3.10 represents the inductance as a function of the delta temperature ΔT for different values of switching frequency:

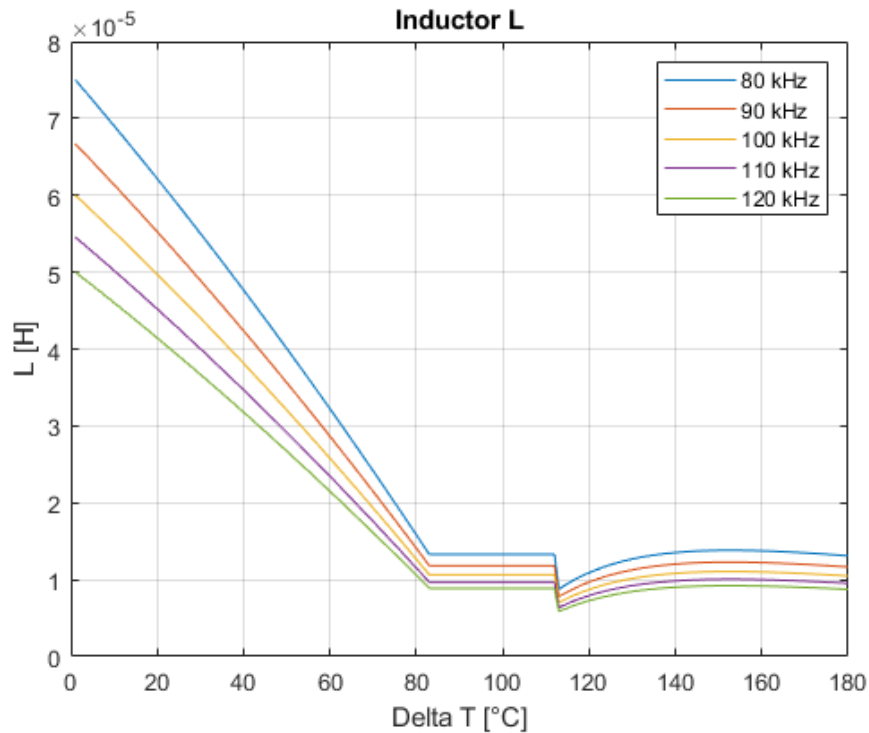


Fig. 3.10 Inductance at several frequencies

Selecting the inductor is the fundamental step for DC-DC design but could be critical because it defines also the operating mode of the converter. Specifying the chosen inductor with L_{dcdc} :

$$L_{dcdc} > L_{Buck} = CCM$$

$$L_{dcdc} < L_{Buck} = DCM$$

The same reasoning is applied to L_{boost} :

$$\begin{aligned} L_{dc} > L_{Boost} &= CCM \\ L_{dc} < L_{Boost} &= DCM \end{aligned}$$

Choosing to stay in CCM mode, it is convenient to pick an inductor with higher values with respect to the ones represented by the plots for each frequency.

For this reasoning and considering also the size and the cost of the component, the inductor chose is **8.2 μ H**. Then the switching frequency is set at **100kHz**.

Duty Cycle Computations

The previous equations illustrates how the inductance depends on duty cycle. The parameter in fact is associated to the selection of the majority of the components and it affects the behavior of the current which flows in the circuit. There are different ways to calculate the duty cycle because of the operation mode in which the converter is working. Table 6 depicts the equations in CCM, instead Table 7 is related to DCM:

Converter	CCM
Buck	$d_{CCM} = \frac{V_{batt}}{V_{mp}}$
Boost	$d_{CCM} = 1 - \frac{V_{mp}}{V_{batt}}$

Table 6

Converter	DCM
Buck	$d_{DCM} = \sqrt{\frac{4L_{dc}f_{sw}I_{out}V_{batt}}{V_{mp}(V_{mp} + 2V_{batt})}}$
Boost	$d_{DCM} = \sqrt{\frac{2L_{dc}f_{sw}I_{out}(V_{batt} - V_{mp})}{V_{mp}}}$

Table 7

At 100 kHz, duty cycles are computed and compared to the value of the input voltage, so to the operating mode of the converter.

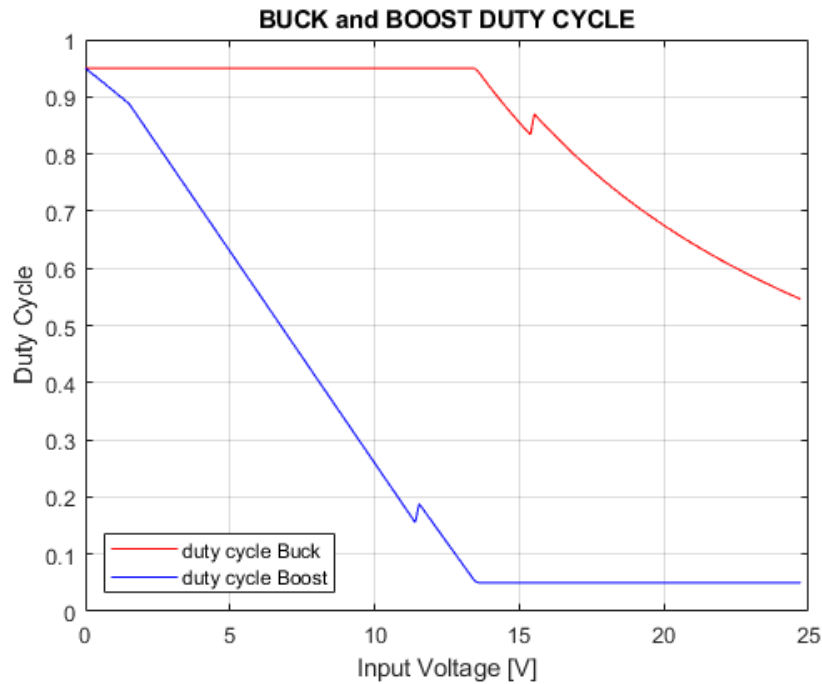


Fig. 3.11 Buck and Boost duty cycles at different input voltage at 100 kHz

The plots in Fig. 3.11 are obtained in Matlab also through some considerations about the distinction between CCM and DCM mode. The criteria used to define the two modes are these:

$$\frac{i_{ripple}}{2I_{mp}} > 1 \Rightarrow Boost DCM \quad (14)$$

$$\frac{i_{ripple}}{2I_{out}} > 1 \Rightarrow Buck DCM \quad (15)$$

The equations express that if the half ripple current of the inductor is greater than the average current of L, the working mode change from CCM to DCM. The aim is to be restricted in the CCM zone.

Capacitors Selection

Both input and output capacitor selection should not be underestimated because they are very stressed components.

For a Buck converter the selection of the input capacitor is critical because it can keep the electromagnetic noise due to the high current which flows from the source.

For a Boost converter, instead, the output capacitor is very stressed. In fact, when the switch is ON, all the current comes from the output capacitor to the load. (Buck converter, differently, delivers always current to the load from the inductor)

In any case some electrical specifications are required when selecting the right capacitors in a DC-DC design [13]:

- RMS current: it is the main parameter to be considered. There are many way to compute it. The general equation, valid for every topology of RMS current is the (16):

$$I_{RMS} = \sqrt{d \frac{I_{min}^2 + I_{min}I_{MAX} + I_{MAX}^2}{3}} \quad (16)$$

If the current is a triangle wave, it is sufficient to follow the equation (17):

$$I_{RMS\Delta} = \frac{I_{peak}}{\sqrt{3}} \quad (17)$$

Another way consists in the RMS itself: Root, Mean and Square the current. Otherwise, one common method is the usage, when possible, of the flat top approximation.

In the Fig. 3.12 the RMS currents of input and output capacitors are revealed, results of Matlab computations. The capacitor have to handle surely 3.5 A.

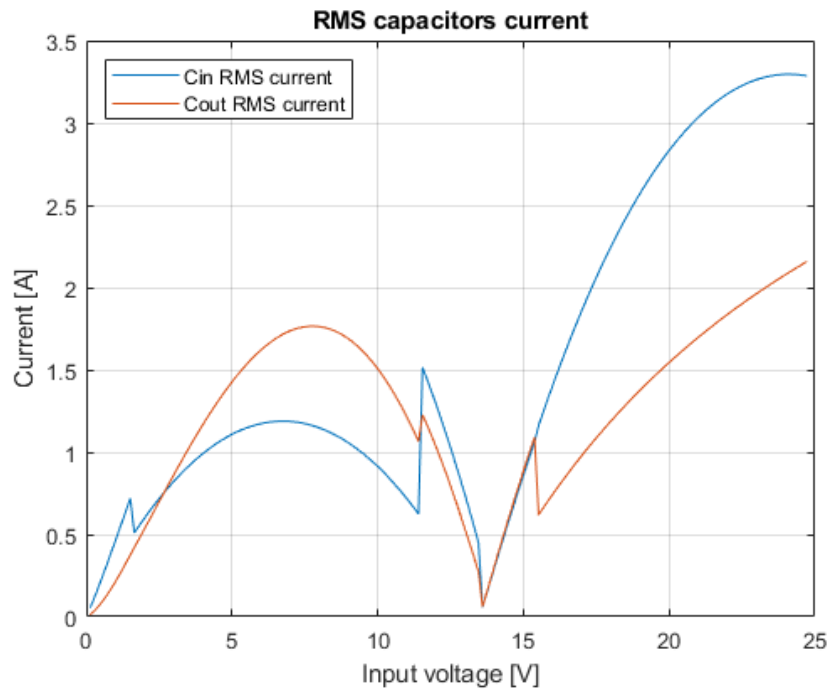


Fig. 3.12 RMS input and output capacitor currents

- Voltage applied on capacitor (from 12 V for the battery to 25 V from the source)
- Capacitor impedance ESR, which has to be as low as possible.

All those considerations lead to select capacitors of **330 μ F** with ESR equal to **41 mOhm**.

Power dissipations and Efficiency

This subsection is related to various computation in order to obtain the general overview of the power dissipations of the DC-DC converter and thus its efficiency. From each components the main losses are computed.

INDUCTOR

The component is characterized by two different power losses: conduction loss and magnetic core loss. Only conduction loss would be considered and it depends on the ESR resistance which is due to the windings of the inductor. ESR value is directly proportional to the inductance; while it is inversely proportional to the case size. As the equations illustrate in Table... the power loss is equivalent to the square of the current and it is not affected by duty cycle. It means that the higher the average current of the inductor, the higher power dissipation [14] and it is well depicted in Fig. 3.13.

Converter	Power dissipated from the Inductor
Buck	$P_L = \left(I_{out}^2 + \frac{I_{ripple}^2}{12} \right) L_{ESR}$
Boost	$P_L = \left(I_{mp}^2 + \frac{I_{ripple}^2}{12} \right) L_{ESR}$
Buck-Boost	$P_L = \left(I_{mp}^2 + \frac{I_{ripple}^2}{12} \right) L_{ESR} + \left(I_{out}^2 + \frac{I_{ripple}^2}{12} \right) L_{ESR}$

Table 8

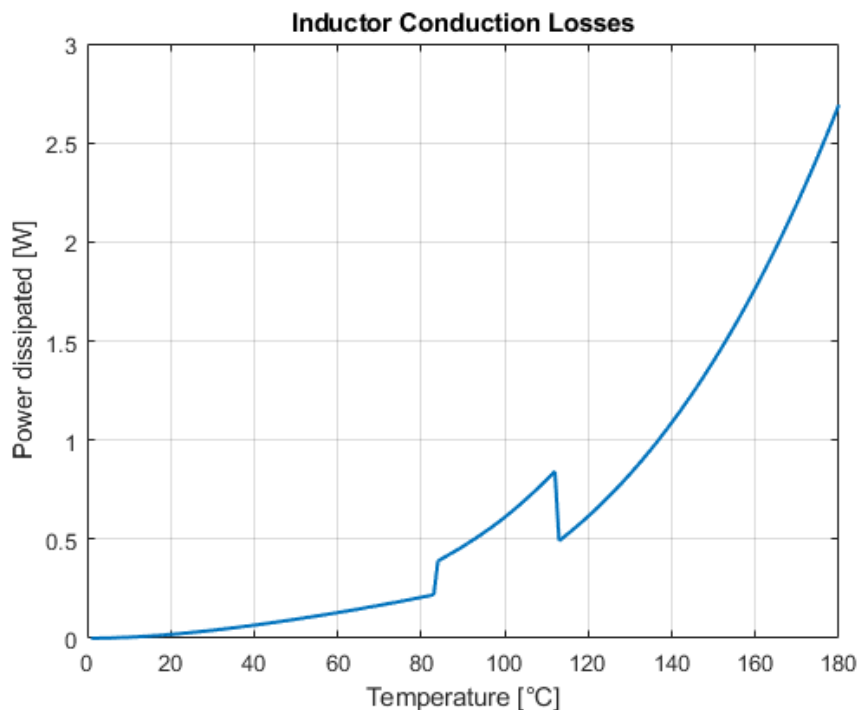


Fig. 3.13 Inductor Conduction Losses

CAPACITORS

The general power dissipation model adopted for the capacitors is defined by the equations...:

$$P_{Cin} = I_{RMS}^2 C_{in} ESR \quad (18)$$

$$P_{Cout} = I_{RMS}^2 C_{out} ESR \quad (19)$$

The losses are calculated multiplying the square of the RMS current with the ESR of the capacitors. The picture below (Fig. 3.14) represents the stress of the input and output capacitors. The first one is more stressed in Buck mode, the output one usually works more in Boost region, but at high temperatures, so high powers, it is stressed as before.

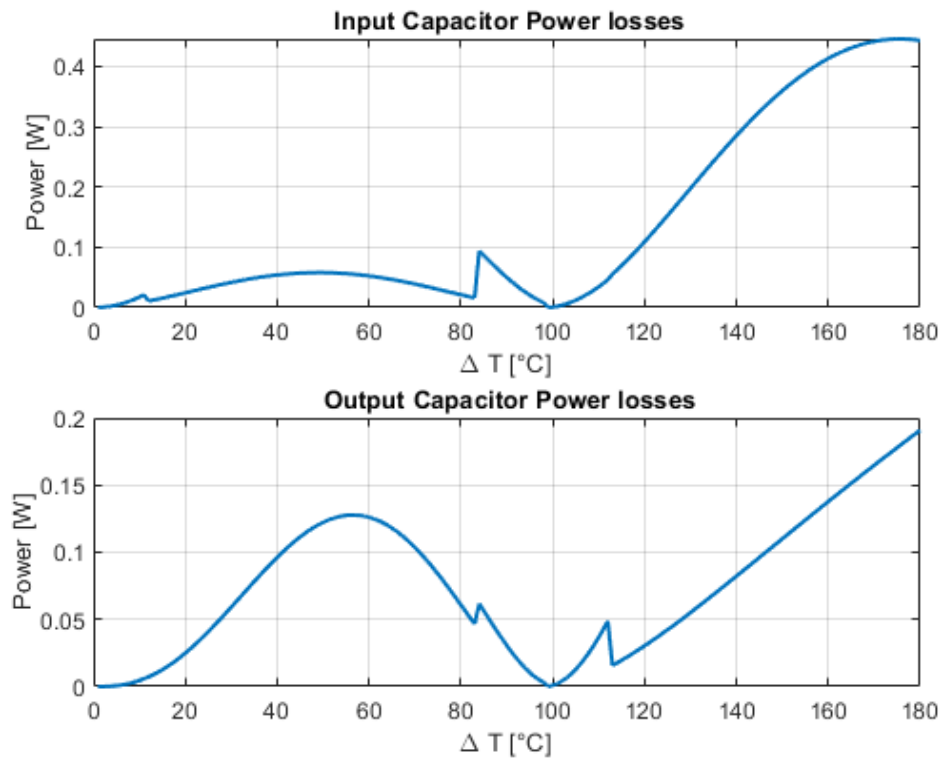


Fig. 3.14 Capacitors Losses

DIODES

The selection of a proper diode depends on some parameters:

- Average current (I_{ave});
- Maximum peak current;
- Maximum reverse voltage (V_f) (which is extracted from the diode characteristic, obtained from the datasheet of the selected component in Fig. 3.15).

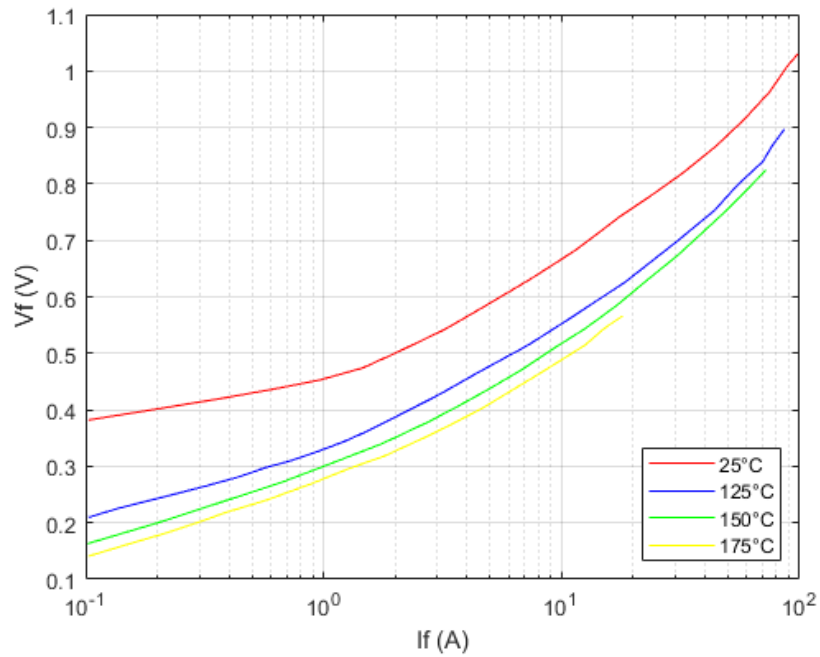


Fig. 3.15 Diodes Characteristic

The characteristic shows the reverse voltage as a function of the instantaneous forward current on a logarithmic graph.

Therefore the power dissipated is then computed:

$$P_{D1} = V_{f1} I_{ave1} \quad (20)$$

$$P_{D2} = V_{f2} I_{ave2} \quad (21)$$

And the result is depicted in the pictures below (Fig 3.16):

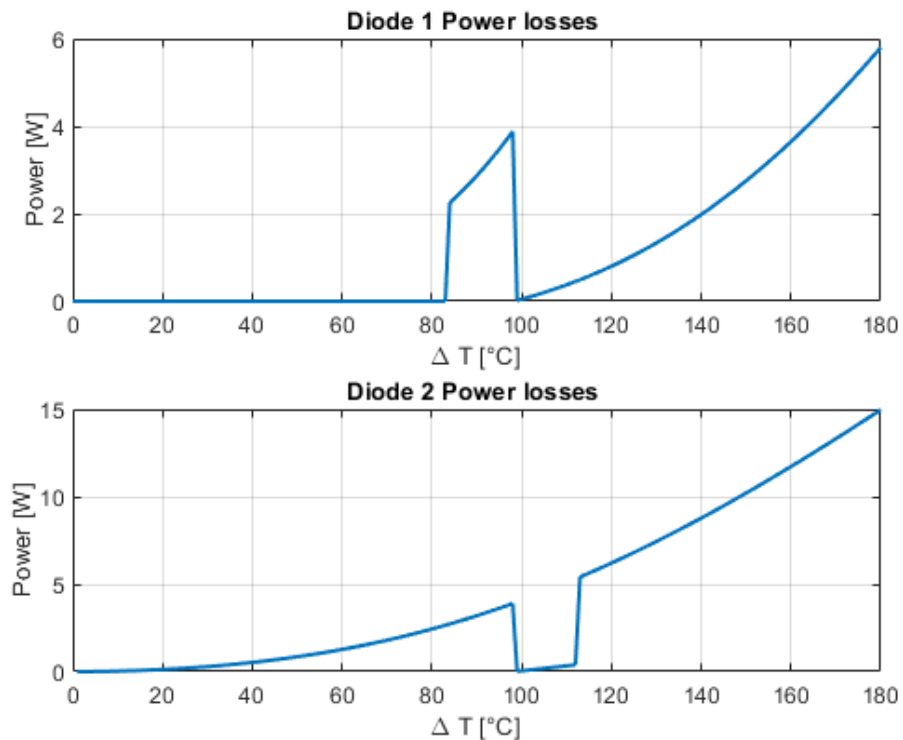


Fig. 3.16 Diodes Losses

The second diode, on the Buck leg, seems to dissipates 15 W, it is extremely high loss just for one diode. A possible solution consist in put two output diodes in parallel, in order to dissipates at least half of this power.

SWITCHES

Switches losses are the most relevant dissipations and they depend mostly on the duty cycle, thus on the different operation modes of the DC-DC converter. In the following tables are represented the power losses equation of both SW1 and SW2, in Buck, Boost or Buck-Boost region. The main dissipations are due to the conduction (duty cycle = 1) and switching (duty cycle = var) conditions. Moreover also the output recharging capacitance (C_{oss}) is considered.

Buck		
LOSSES	SW1	SW2
Conduction loss	$P_{con} = \left(I_{out}^2 + \frac{I_{ripple}^2}{12} \right) R_{dson} d_{Buck}$	$P_{con} = 0$
Switching loss	$P_{sw} = V_{mp} I_{out} (t_R + t_F) \frac{f_{sw}}{2}$	$P_{sw} = 0$
Output Capacitance C_{oss} loss	$P_{Coss} = C_{oss} V_{mp}^2 \frac{f_{sw}}{2}$	$P_{Coss} = 0$

Table 9

Boost		
LOSSES	SW1	SW2
Conduction loss	$P_{con} = \left(I_{out}^2 + \frac{I_{ripple}^2}{12} \right) R_{dson} d_{Boost}$	$P_{con} = \left(I_{mp}^2 + \frac{I_{ripple}^2}{12} \right) R_{dson} d_{Boost}$
Switching loss	$P_{sw} = 0$	$P_{sw} = V_{batt} I_{mp} (t_R + t_F) \frac{f_{sw}}{2}$
Output Capacitance C_{oss} loss	$P_{Coss} = 0$	$P_{Coss} = C_{oss} V_{batt}^2 \frac{f_{sw}}{2}$

Table 10

Buck in Buck-Boost region		
LOSSES	SW1	SW2
Conduction loss	$P_{con} = \left(I_{out}^2 + \frac{I_{ripple}^2}{12} \right) R_{dson} d_{Buck}$	$P_{con} = \left(I_{mp}^2 + \frac{I_{ripple}^2}{12} \right) R_{dson} d_{Buck}$
Switching loss	$P_{sw} = V_{mp} I_{out} (t_R + t_F) \frac{f_{sw}}{2}$	$P_{sw} = V_{batt} I_{mp} (t_R + t_F) \frac{f_{sw}}{2}$
Output Capacitance C_{oss} loss	$P_{Coss} = C_{oss} V_{mp}^2 \frac{f_{sw}}{2}$	$P_{Coss} = C_{oss} V_{batt}^2 \frac{f_{sw}}{2}$

Table 11

Boost in Buck-Boost region		
	SW1	SW2
Conduction losses	$P_{con} = \left(I_{out}^2 + \frac{I_{ripple}^2}{12} \right) R_{dson} d_{Boost}$	$P_{con} = \left(I_{mp}^2 + \frac{I_{ripple}^2}{12} \right) R_{dson} d_{Boost}$
Switching Losses	$P_{sw} = V_{mp} I_{out} (t_R + t_F) \frac{f_{sw}}{2}$	$P_{sw} = V_{batt} I_{mp} (t_R + t_F) \frac{f_{sw}}{2}$
Coss	$P_{Coss} = C_{oss} V_{mp}^2 \frac{f_{sw}}{2}$	$P_{Coss} = C_{oss} V_{batt}^2 \frac{f_{sw}}{2}$

Table 12

As seen from the tables, the Buck-Boost region is divided in two parts, evaluating the different duty cycles whether up or down from the battery reference (13.5 V).

Following pictures shows the Matlab losses computation results:

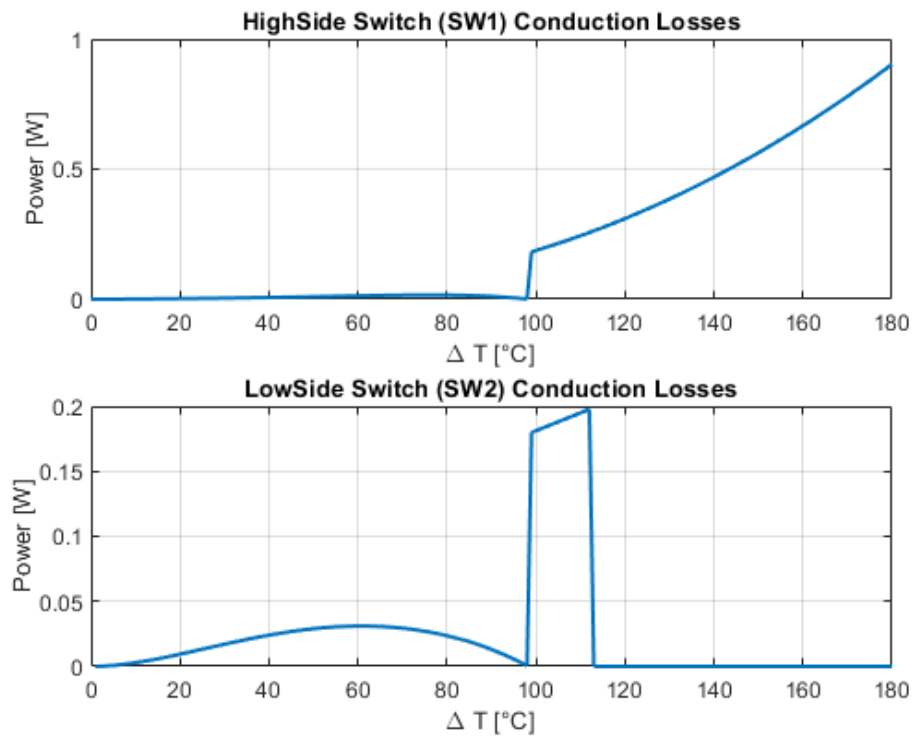


Fig. 3.17 Switches Conduction Losses

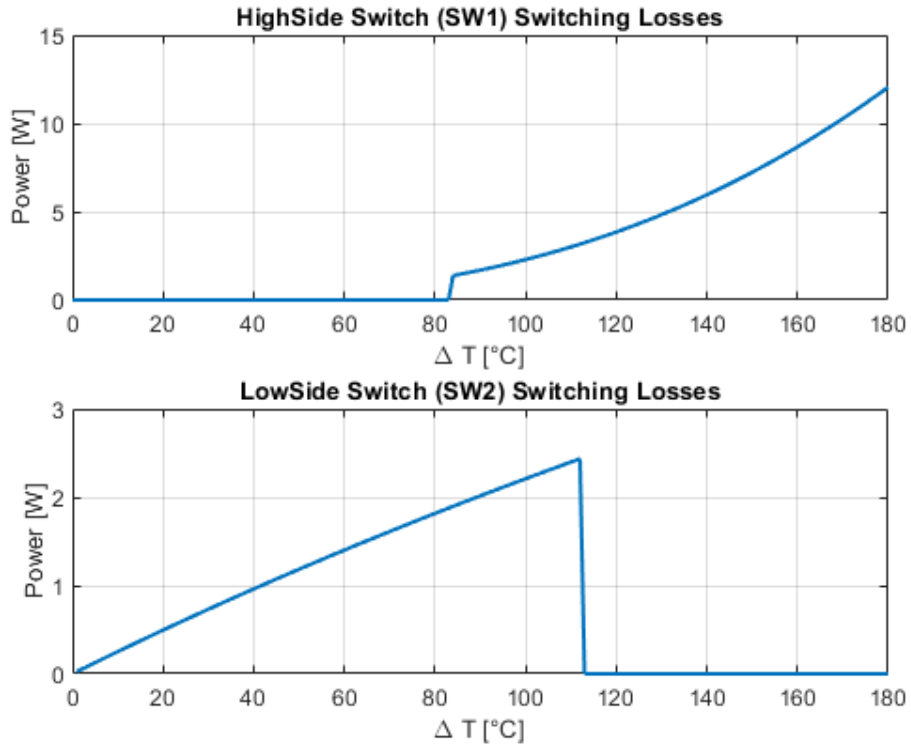


Fig. 3.18 Switches Switching Losses

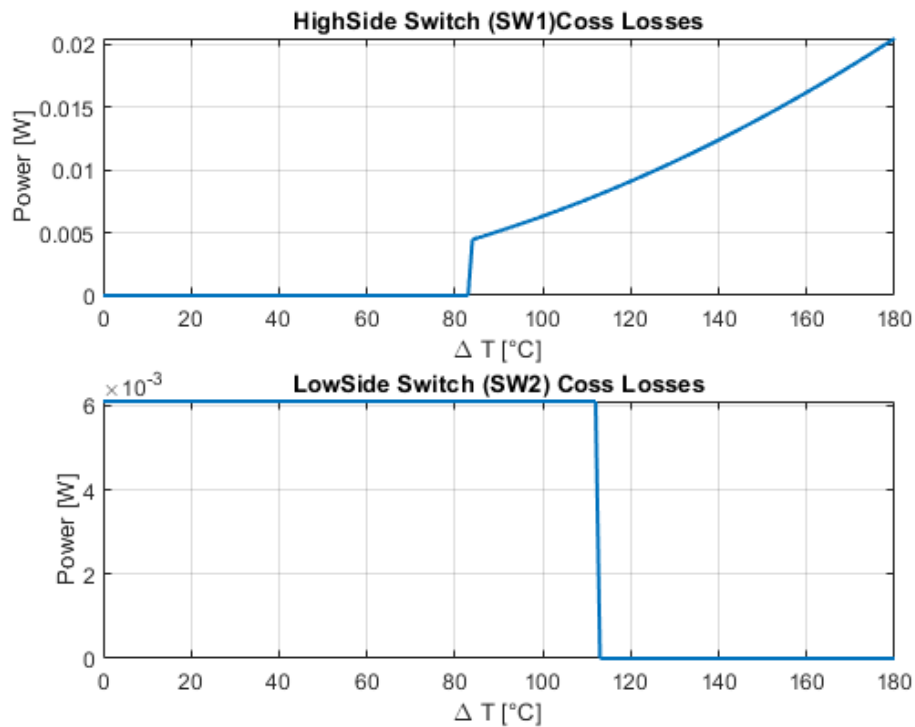


Fig. 3.19 Switches Capacitance Losses

Additionally another value has to be esteemed: the gate charging loss in equation (22):

$$P_{gate} = Q_{gs} V_{gs} f_{sw} * 2 \quad (22)$$

In conclusion, the amount of the overall power dissipation of the DC-DC converter is made of all the previous contributions, as depicted in the equation (23):

$$P_{diss} = P_L + P_{Cin} + P_{Cout} + P_{D1} + P_{D2} + P_{con1} + P_{sw1} + P_{Coss1} + P_{con2} + P_{sw2} + P_{Coss2} + P_{gate}$$

Knowing that

$$P_{out} = P_{in} - P_{diss} \quad (24)$$

It is possible to calculate the efficiency:

$$\eta = \frac{P_{out}}{P_{in}} 100 \quad (25)$$

And to observe the final values on the figures of Fig. 3.20.

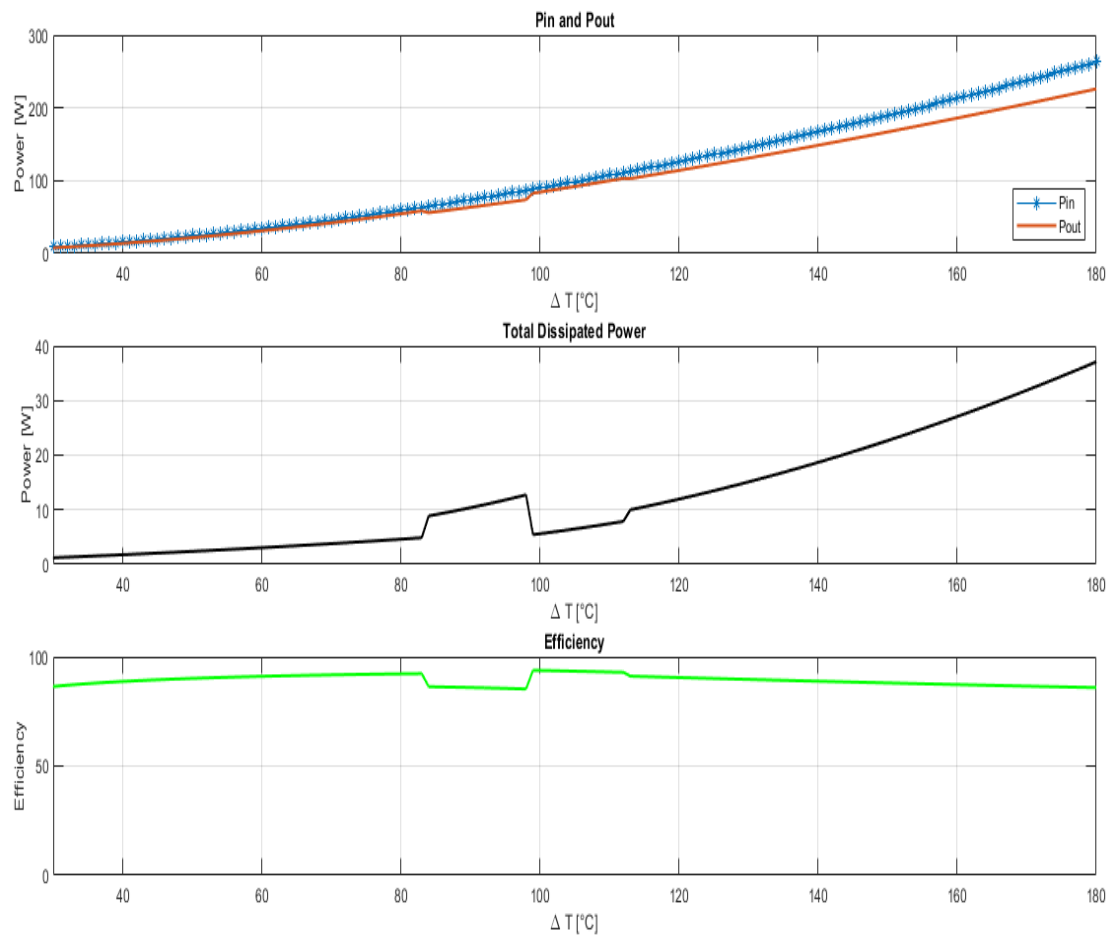


Fig. 3.20 Pin/Pout, Dissipated Power and Efficiency

Control algorithms and simulations

MPPT, ALGORITHMS AND IMPLEMENTATIONS

Maximum Power Transfer Theorem

The primary objective of the project is to realize a device capable to recharge the battery through the heat dissipated from the exhaust of a vehicle. To ensure enough energy and to guarantee the best performance of the entire system, it is necessary to transfer the maximum power from the TEG to the load. As seen in the previous chapter, the TEG can be definitely modelled as a voltage generator with a resistor in series, which depends on the material used for the TE modules. Therefore it is possible to apply the maximum power transfer theorem. It states that the maximum power can be transferred when the total resistive value of the load is equal to the internal resistance of the source. The output voltage and current of the TEG reveal a linear relation between them. The output power has a quadratic behavior, a parabolic trajectory with a distinguishable maximum point. (Fig.4.1) Those values are functions of the temperature difference of the TE modules.

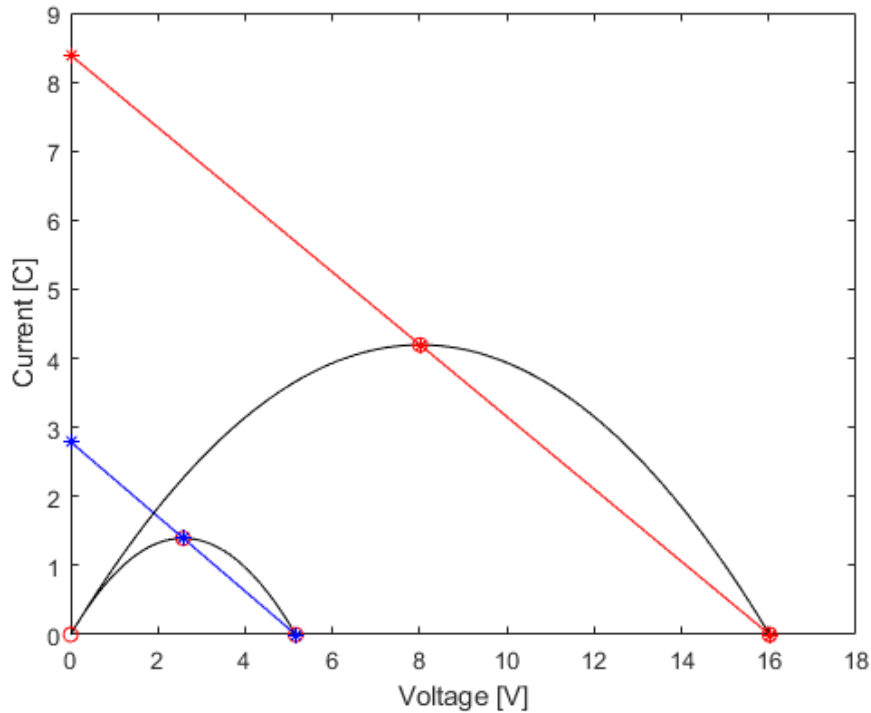


Fig. 4.1 Power parabolic behavior - Matlab

For each curve at given temperature there is one maximum power point, consequently, Maximum Power Point Tracking Techniques (MPPT) have to be developed, modified and applied to our system.

For any specific condition, the MPPT can give a different reference, important for the DC-DC control implementation.

The literature illustrates two main fundamental algorithms: P&O (Perturbation and Observation) and IC (Incremental Conductance) algorithms. They will be described briefly in these pages, because from them the modified algorithm would be computed.

Perturb and Observe (P&O) algorithm

Among the MPPT methods, P&O represents the simplest algorithm to enhance the performance in a simple way. The basic procedure lies in perturbing the voltage or the current of the TEG and then observing the results on the power generated [15].

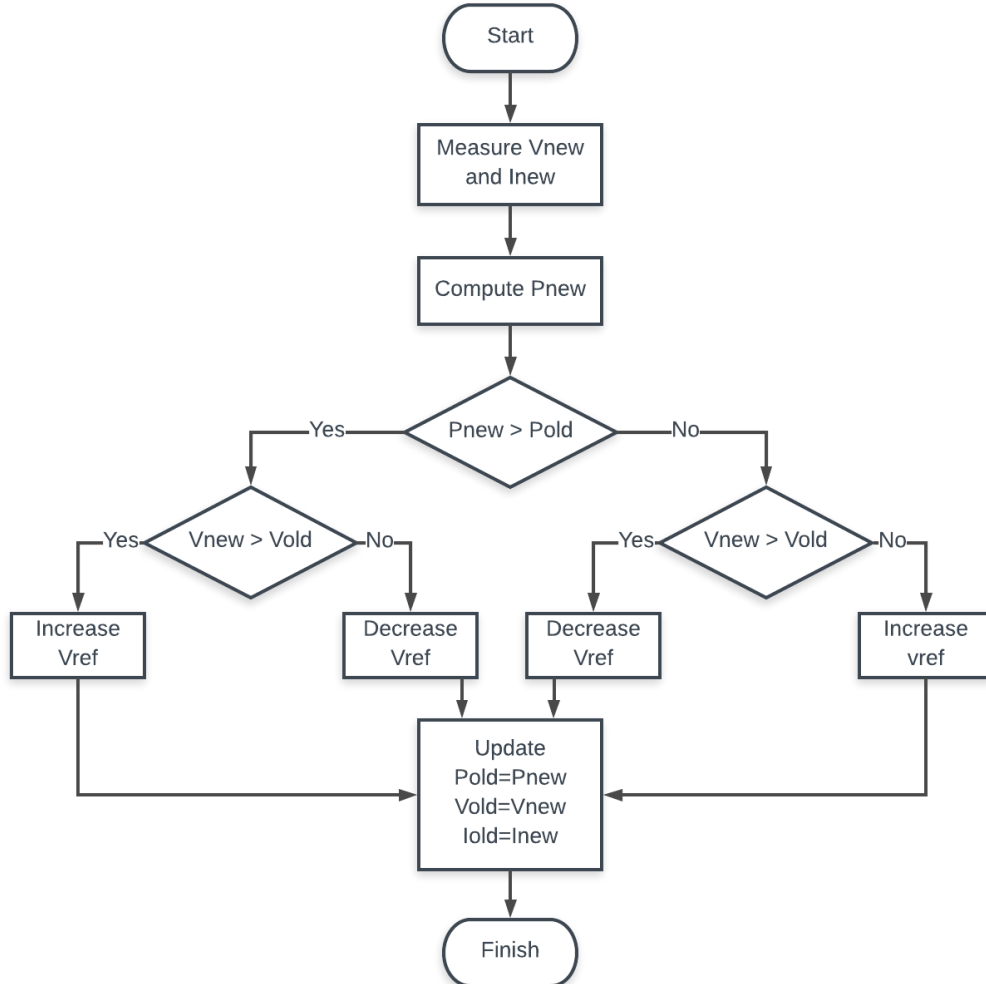


Fig. 4.2 P&O flowchart

The Fig 4.2 depicts the flowchart exemplification of P&O algorithm, which is summarize in the equations below:

$$\frac{dP}{dV} = 0 = MPP$$

$$\frac{dP}{dV} > 0 = \text{left of MPP}$$

$$\frac{dP}{dV} < 0 = \text{right of MPP}$$

For each cycle the previous power and voltage are compared to the new one; the effect consists in decreasing or increasing continuously the voltage reference. Thus, the working point is incessantly moving toward the MPPT to guarantee the maximum performance.

Instead of having a reference voltage, it is possible to have a duty cycle reference and apply it directly to the control of the DC-DC converter.

The behavior of the algorithm could be improved by changing some specifications, for example the step of the reference (voltage or duty cycle) or the sampling period.

Incremental Conductance (IC) algorithm

The algorithm is developed to improve the previous one in some limitations, especially convergence speed and steady-state error [16]. As shown by the diagram of Fig. 4.3 and the equations of the box, it is used the concept of the derivative of the power. The result could be seen in a faster response and precision.

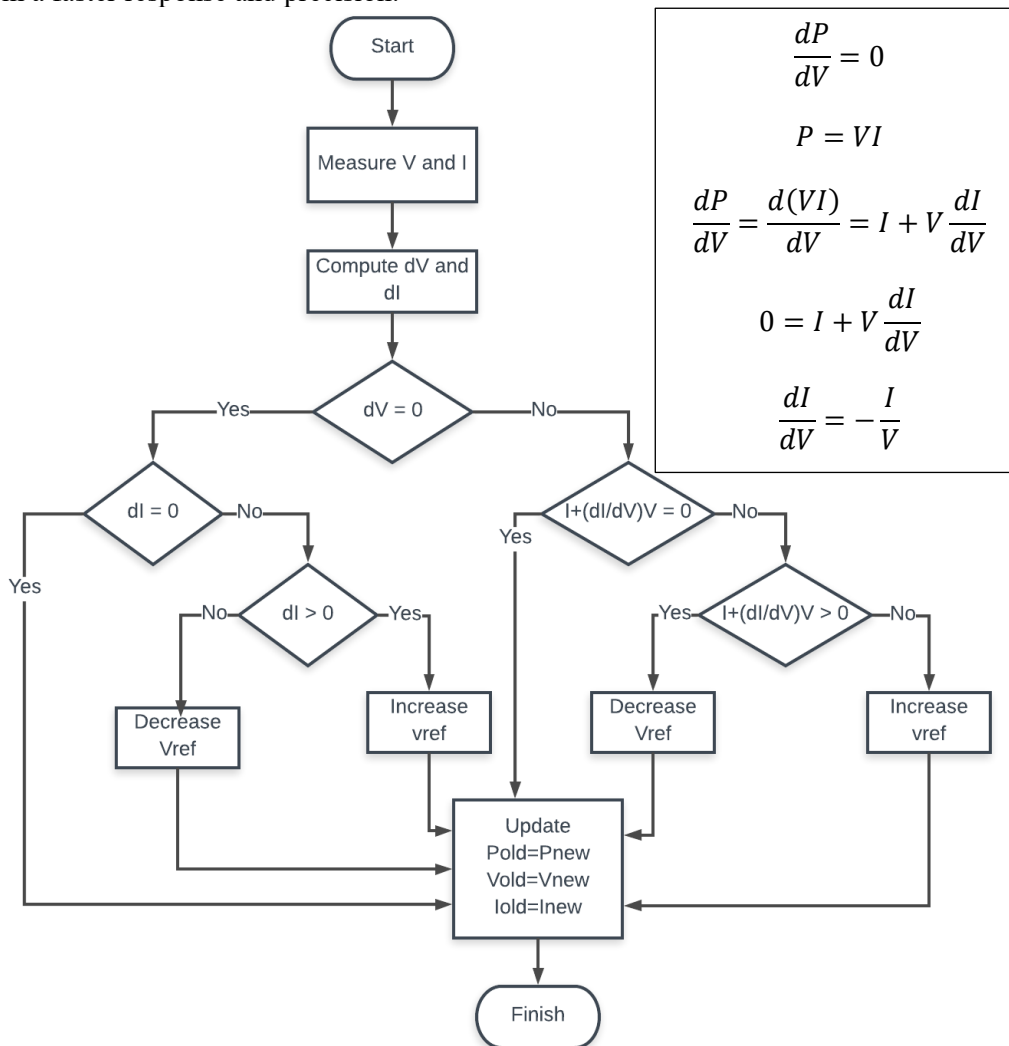


Fig. 4.3 IC flowchart

When:

$$\frac{dI}{dV} = -\frac{I}{V} = MPP$$

$$\frac{dI}{dV} > -\frac{I}{V} = \text{left of MPP}$$

$$\frac{dI}{dV} < -\frac{I}{V} = \text{right of MPP}$$

The usage of those equations permits to choose the best following operating point.

Modified algorithms and implementation

As shown in the Fig. 4.4 the Simulink environment is made by three blocks: TEG block (green), Measuring block (red) and MPPT block (blue). Instead of having directly the DC-DC converter, the load of the system is represented by a variable resistor. Therefore, the modified MPPT algorithms would give a resistance reference, from which in next chapters a current reference will be developed for the current control loop.

Now it is important to affirm the correctness of the algorithms and it is made by representing the converter as a simple resistor.

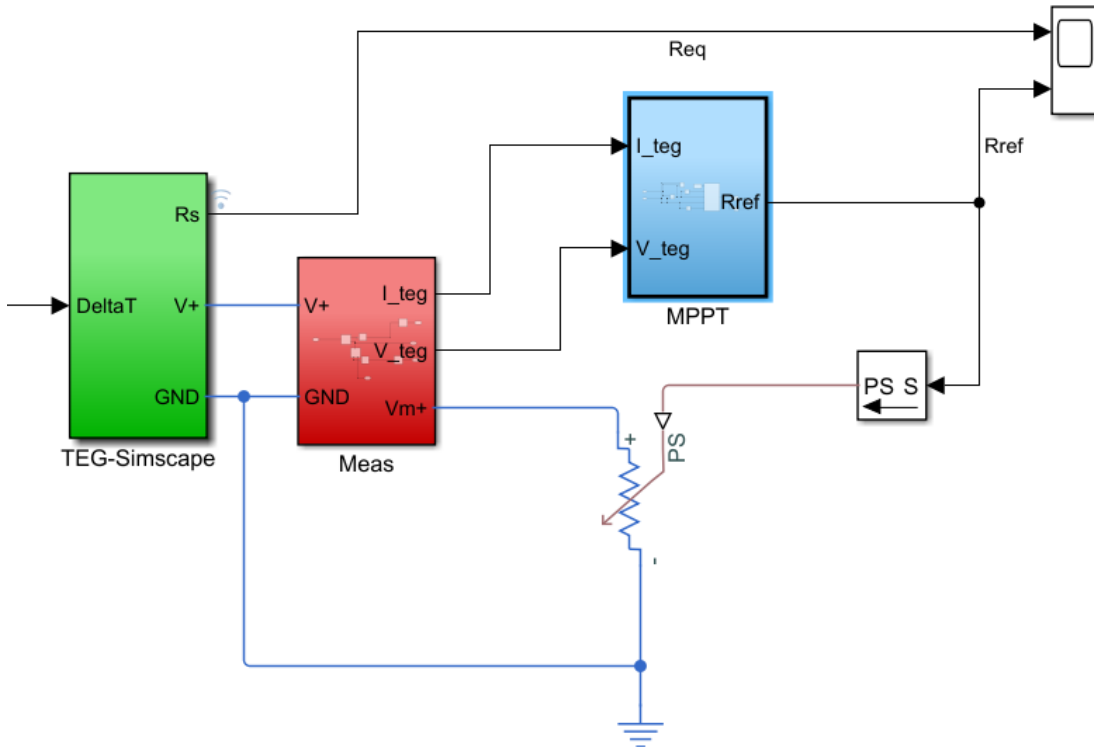


Fig. 4.4 MPPT Simulink simulation

The modified algorithms realized are three and they are based on the model of the P&O and IC algorithms.

P&O_1 modified algorithm

The first algorithm is well depicted in the flowchart of Fig. 4.5. By measuring the power and the voltage of the TEG, it compares the new with the old values and the result is just a step up or down of the resistance. It is always a perturbation because the resistance cannot be constant. The precision of this model is confirmed when, as the maximum power theorem states, the value of the variable resistor reaches the source resistance.

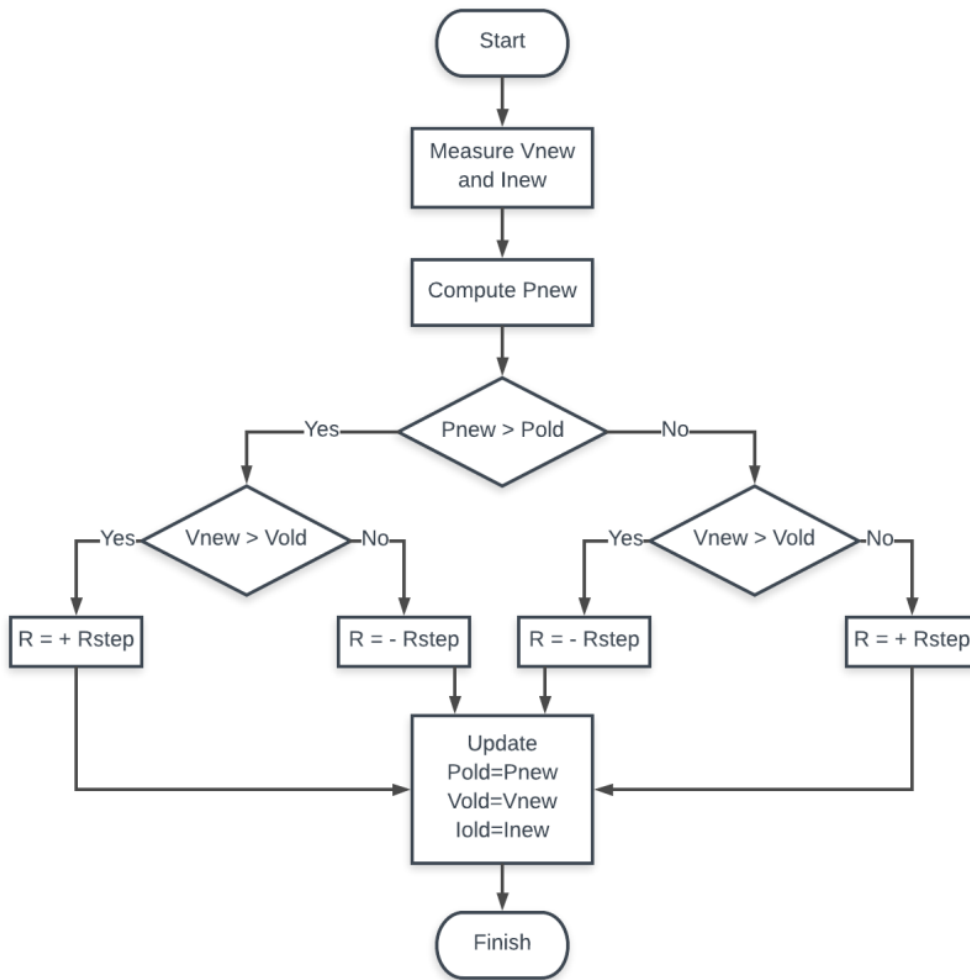


Fig. 4.5 P&O_1 modified flowchart

The Matlab function adopted is illustrated in the figure Fig. 4.6

```

function R = P_O_func(R_step, P_old, P_new, V_new, V_old)

if (P_new > P_old)

    if (V_new > V_old)
        R = + R_step;
    else
        R = - R_step;
    end
else
    if (V_new > V_old)
        R = - R_step;
    else
        R = + R_step;
    end
end
end
    
```

Fig. 4.6 P&O_1 Matlab algorithm

P&O_2 modified algorithm

The flowchart which explained graphically the second modified algorithm is in Fig. 4.7. Because of the resistance reference could not be constant, it would be equal to the positive or negative value of the step for each cycle. For example, if the new power is higher than the old one and if the previous resistance have been increased, it means that the maximum power point is not reached yet. Hence it is necessary to reduce the current (thus to have higher resistance) and to increase the voltage.

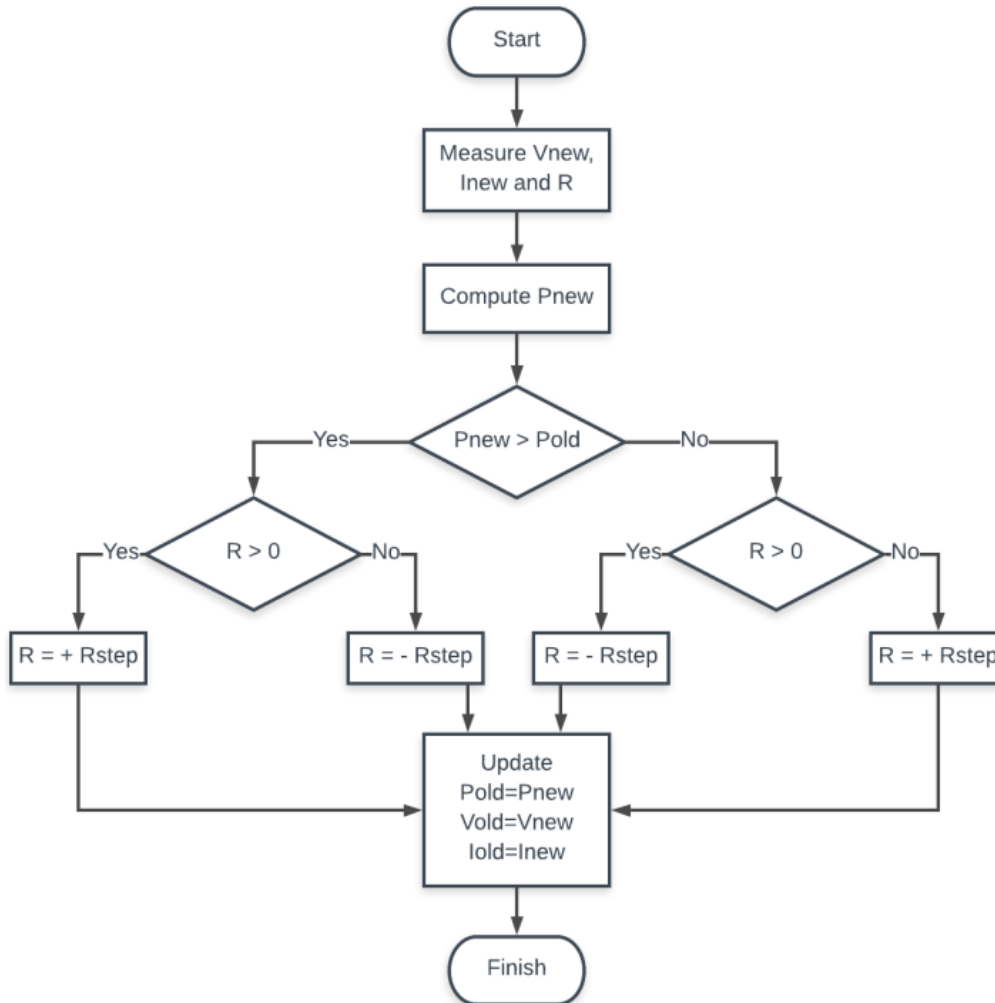


Fig. 4.7 P&O_2 modified flowchart

As for the previous algorithm, below there is the Matlab algorithm (Fig. 4.8):

```
function R = P_O_modify(R_step, P_old, P_new, R)

if (P_new > P_old)

    if (R > 0)
        R = + R_step;
    else
        R = - R_step;
    end

else

    if (R > 0)
        R = - R_step;
    else
        R = + R_step;
    end

end
```

Fig. 4.8 P&O_2 Matlab algorithm

IC modified algorithm

The third modified algorithm is just an adjustment of the IC one. The principle again lies on the concept of the maximum power. If the reached point is not considered the maximum the reference has to move. The step is positive or negative with respect to the new value of voltage. The relative flowchart and Matlab function are illustrated below in Fig. 4.9 and Fig. 4.10.

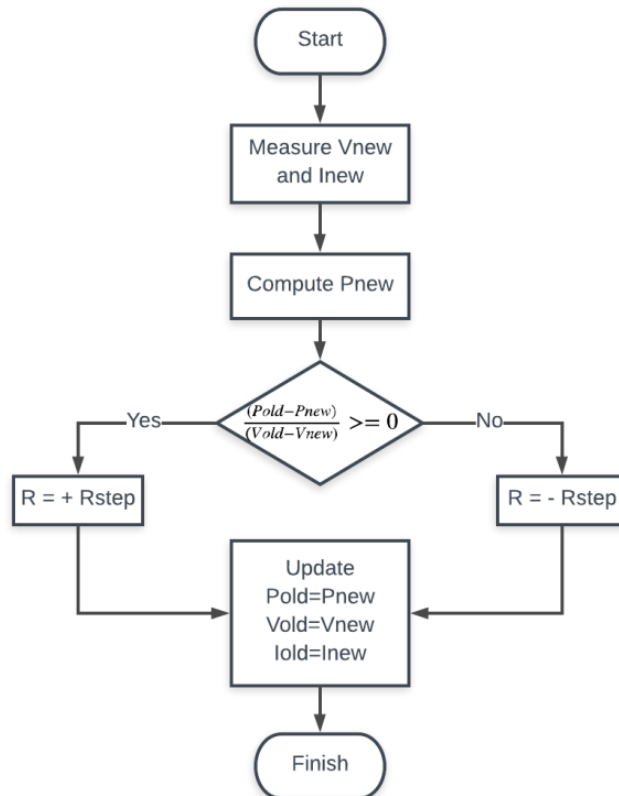


Fig. 4.9 IC modified flowchart

```

function R = P_O_modify(R_step, P_old, P_new, V_new, V_old)

if ((P_old-P_new)/(V_old-V_new)) >= 0

    R = + R_step;

else

    R = -R_step;

end
    
```

Fig. 4.10 IC modified Matlab algorithm

This algorithm would be applied to the control. Given a ramp reference, the simulations in Simulink (Fig. 4.11 and Fig. 4.12) shows that after 2 ms the obtained resistance follows the source one.

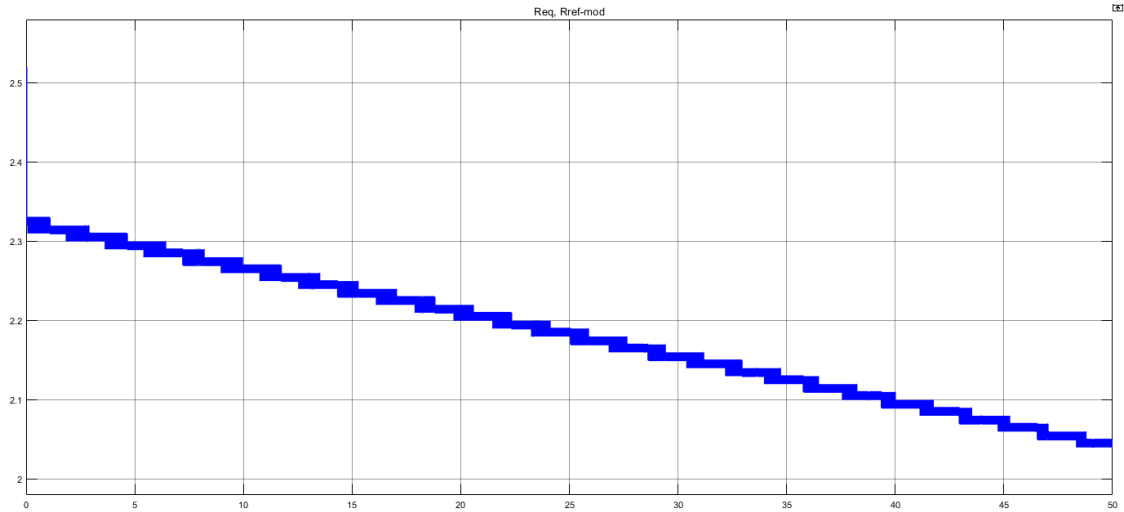


Fig. 4.11 Simulink simulation 50 sec IC modified

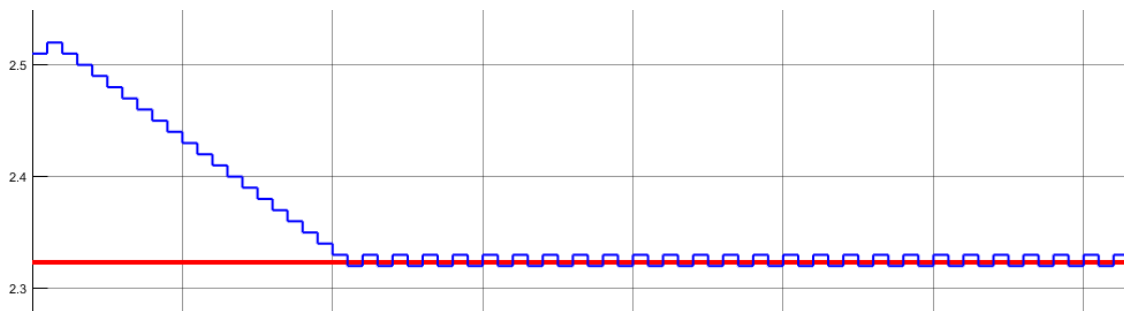


Fig. 4.12 Simulink simulation 2 millisecc IC modified

From the resistance, by applying simple calculations, it is easy to acquire a current reference through equation (26):

$$I_{ref} = \frac{V_{mp}^2}{RV_{batt}} \quad (26)$$

CONTROL DESIGN

To ensure a proper control of the system, it is necessary to control output current and voltage through feedbacks. In order to make it, the right transfer functions should be obtained. First of all the duty cycle represents the control input of the converter, voltage and current are the outputs (Fig. 4.13):



Fig. 4.13 Basic control principle scheme

The picture above depicts two inputs: Buck and Boost duty cycles. In fact the basis of the control of the present system, lies on the differentiation of the two converters. This is due to the aim to simplify the control algorithms, transfer functions and simulations.

The DC-DC converter is made of non-linear element, such as switches and diodes. Therefore the DC-DC is a Non Linear Time Variant system (NLTV). Transfer functions can be found only with stable systems [9].

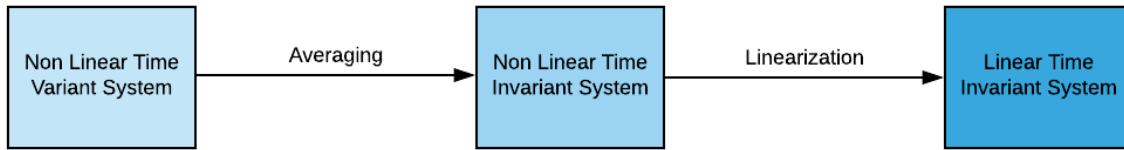


Fig. 4.14 From NLTV to LTI system scheme

As shown in the Fig. 4.14, the model needs to be averaged and then linearized, for this reason it is used the state space averaging method (known also as Middlebrook method).

The transfer functions for each converter related to the current loop are shown in Table 13, the others related to the voltage loop in Table 14:

Mode	Current Loop ($G = \frac{i_{out}}{d}$)
Buck	$G_{di} = \frac{R(1 + sC_{out}ESR)}{(1 + sRC_{out})} \quad (20)$
Boost	$G_{di} = \frac{R(1-d)}{2} * \frac{\left(1 - \frac{sL_{dc}dc}{R(1-d)^2}\right) * (1 + sC_{out}ESR)}{\left(1 + \frac{sRC_{out}}{2}\right)} \quad (22)$

Table 13

Mode	Voltage Loop ($G = \frac{v_{out}}{d}$)
Buck	$G_{dv} = \frac{V_{mp}(1 + sC_{out}ESR)}{\left(1 + \frac{sL_{dc}dc}{R} + s^2L_{dc}dcR\right)} \quad (21)$
Boost	$G_{dv} = \frac{V_{mp}}{(1-d)^2} * \frac{\left(1 - \frac{sL_{dc}dc}{R(1-d)^2}\right) * (1 + sC_{out}ESR)}{\left(1 + \frac{sRL_{dc}dc}{(1-d)^2} + \frac{s^2L_{dc}dcC_{out}}{(1-d)^2}\right)} \quad (23)$

Table 14

CONTROL STRATEGIES AND SIMULINK ARCHITECTURES

The initial control approach consists in a dual control loop, made of an inner current loop and an external voltage loop, as depicted in Fig. 4.15

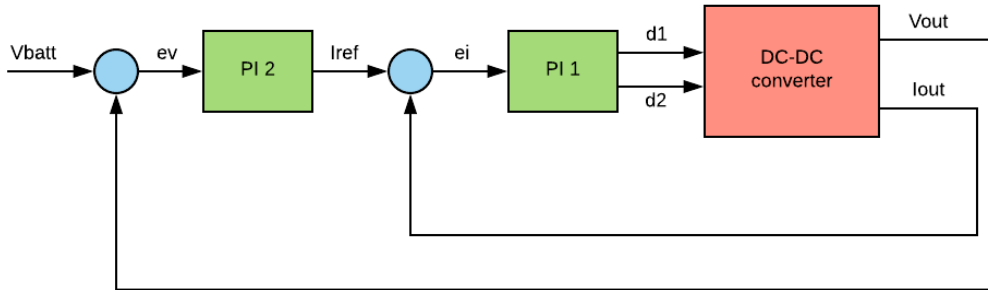


Fig. 4.15 Dual control loop scheme

The controller used in the simulations are PI controllers, which are characterized by the below equation:

$$P = Kc \left(1 + \frac{Ki}{s} \right) \quad (27)$$

Defining with P2 the function of the external controller, with P1 the function of the current controller; the resulting control transfer functions are achieved:

For the Current Loop

$$TF1 = \frac{P1 * G_{di}}{1 + P1 * G_{di}} \quad (28)$$

For the Voltage Loop

$$TF2 = \frac{P2 * P1 * G_{dv}}{1 + P2 * P1 * G_{dv}} \quad (29)$$

The right proportional and integral parameter, Kc and Ki, are the objectives for a proper control. Because of the complexity of the converter and of the control itself, the procedure should be organized in steps:

- Step1: divide the control study in two separated parts: one for Buck and the other for Boost converter;
- Step2: guarantee an accurate and fast current control for each converters;
- Step3: develop the voltage control, slower than the current one, for each converter;
- Step5: compare the different parameters, find the right working zone for both converters and choose the final Kc and Ki.

First of all, it is important to ensure a fast and reactive behavior of the initial part of all the control strategies: the current loop.

First Control Strategy: Current Loop

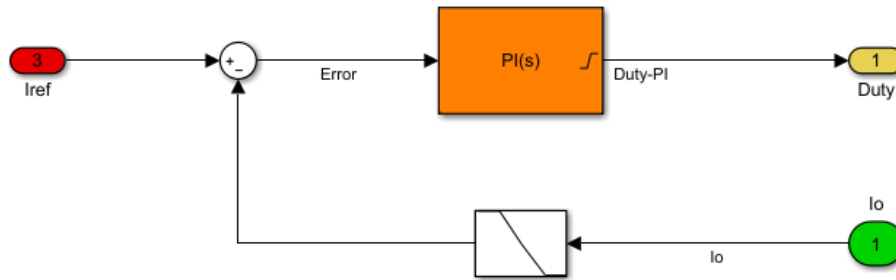


Fig. 4.16 Current Control Loop

The picture in Fig. 4.16 depicts the current control loop in the Simulink environment. The input (in red) is a current and initially it is a constant reference. The output current which comes from the output of the DC-DC (in green) is filtered and then compared to the reference. The difference, thus the error between them is the input of the controller. The output of the PI (in yellow) represents the duty cycle of the converter.

For Buck converters the parameters selected for the PI controller are:

$$K_{CBuck} = 0.01$$

$$K_{iBuck} = f_{pBuck} = \frac{1}{2\pi R C_{out}} = 689.3953$$

The integral parameter is chosen equal to one pole of the transfer function of the Buck converter. The Fig. 4.17 illustrates how the output current follows the reference, it is zoomed in Fig. 4.18.

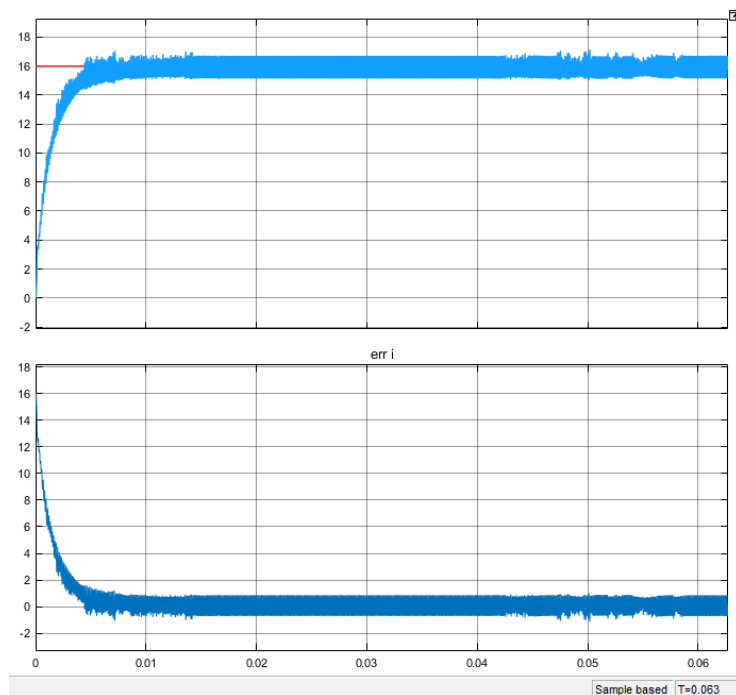


Fig. 4.17 Ref/output current and current error Simulink (Buck)

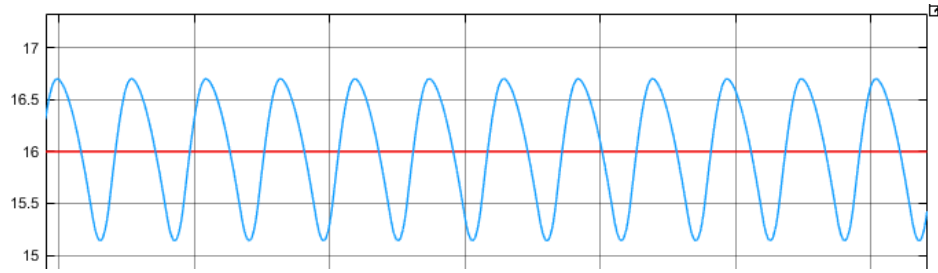


Fig. 4.18 Zoom of Ref/output current (Buck)

For Boost converters the parameters selected for the PI controller are:

$$Kc_{Boost} = 1$$

$$Ki_{Boost} = fp_{Boost} = \frac{1}{2} = 1378.79$$

The result is shown in the figures below (Fig. 4.19 and Fig. 4.20)

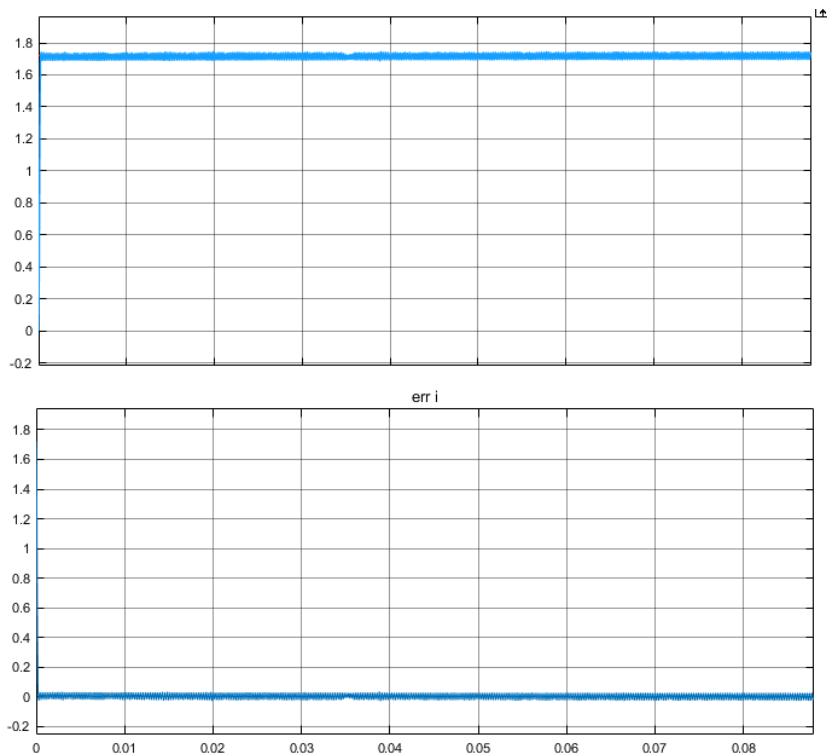


Fig. 3.19 Ref/output current and current error Simulink (Boost)

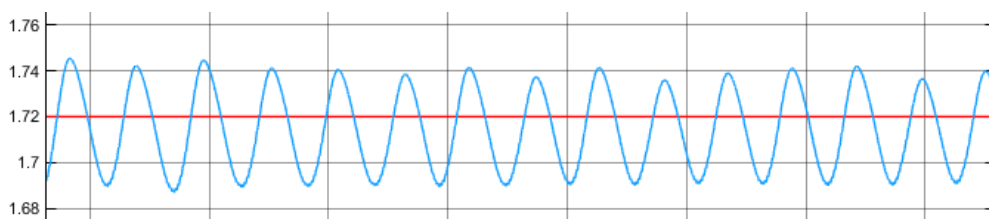


Fig. 4.20 Zoom of Ref/output current (Boost)

Second Control Strategy: Dual Loop

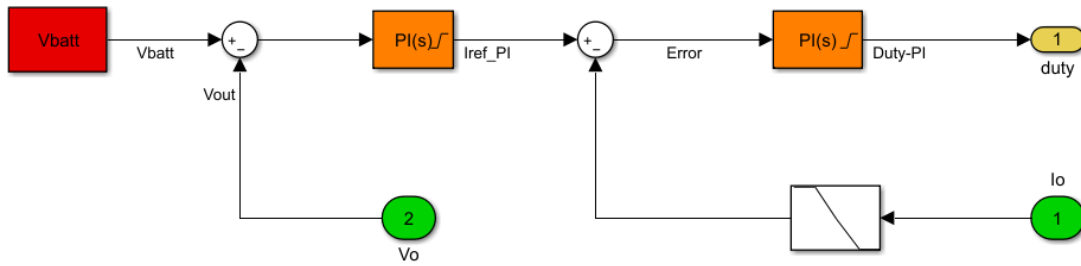


Fig. 4.21 Dual Control Loop

The second strategy is based on the complete dual control loop. The inner current loop, now, follows an external voltage loop, hence the output of the first PI controller (in orange) gives a current reference input for the second PI. The output voltage is compared to the battery voltage, the error would be the input of the voltage PI.

Choosing the parameter below

$$K_{ci} = 0.05$$

$$K_{ii} = 1000$$

For the PI current controller, and

$$K_{cv} = 2$$

$$K_{iv} = 10$$

For the PI voltage controller, with $\Delta T=180^{\circ}\text{C}$, in the Simulink environment the results obtained are illustrated in the following plots.

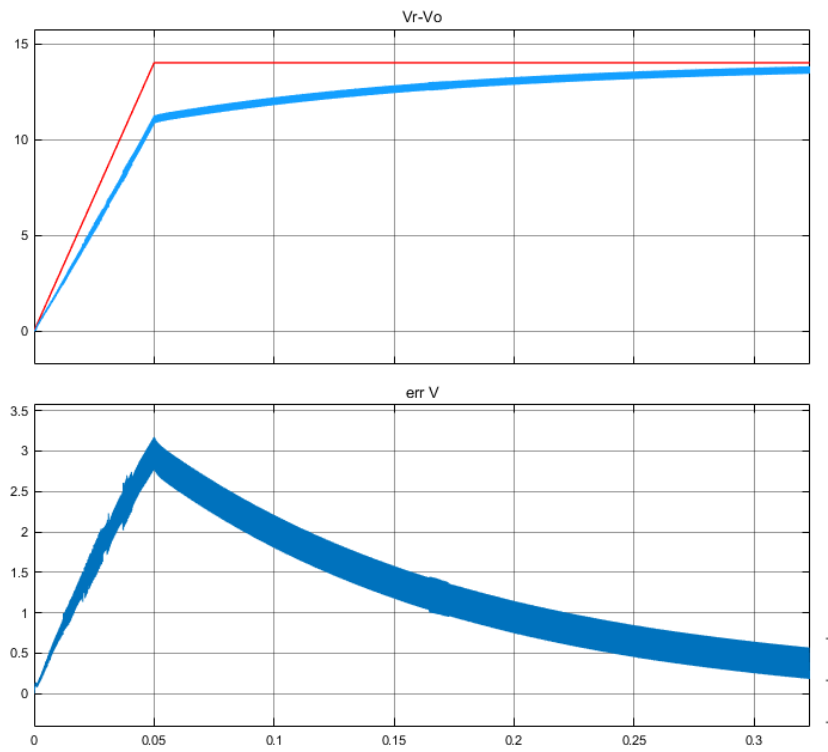


Fig. 4.22 Reference/output voltage and voltage error Simulink dual loop

Fig.4.22 compares the voltage reference (the red ramp) with the output voltage, which after some seconds can reach the voltage reference (chosen at 15 V). In Fig. 4.23 there is the current comparison. It is satisfying, the output current is fast in following the red reference. Moreover it is less oscillating than the reference.

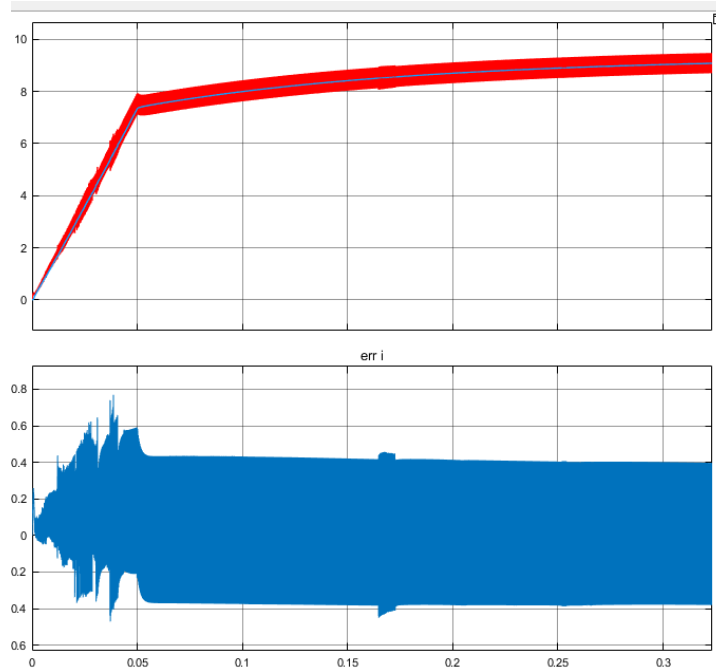


Fig. 4.23 Reference/output current and current error Simulink dual loop

Third Control Strategy: MPPT + Current Loop

The third control approach is made of MPPT and the current control loop (Fig.4.24).

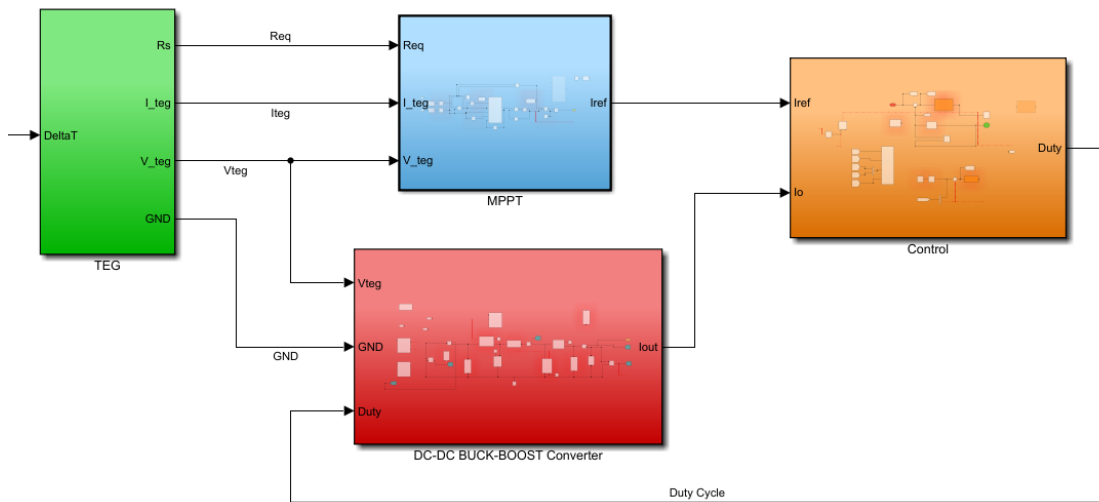


Fig. 4.24 MPPT control + Current Loop Simulink

The explanation requires the description of the different tool which are used in the Simulink environment:

- The TEG is the left green scheme and it is defined by the temperature gradient ΔT . Its output current and voltage go directly to supply the DC-DC and to the MPPT block. In addition, also the equivalent resistance value is sent to the MPPT, in order to perform the algorithm;

- The MPPT block is the blue one. Inside the IC modified algorithm is implemented and adjusted with few calculations to obtain a reference current instead of just a resistance;
- The result of the MPPT would be the input of the current control loop, represented by the orange block. Among the inputs of the control there is also the output current of the converter, in order to compare it to the MPPT reference.
The output is the duty cycle for the high side (Buck leg) or the low side switch (Boost leg);
- The DC-DC converter is represented by the red block. It receives the parameters from the TEG and the duty cycle from the control block.

The MPPT algorithm applied is the IC modified one and the parameters selected for the PI current controller are always:

$$Kc = 0.05$$

$$Ki = 1000$$

In the figures below there are some interesting results after the simulation ran at $\Delta T = 180^\circ\text{C}$.

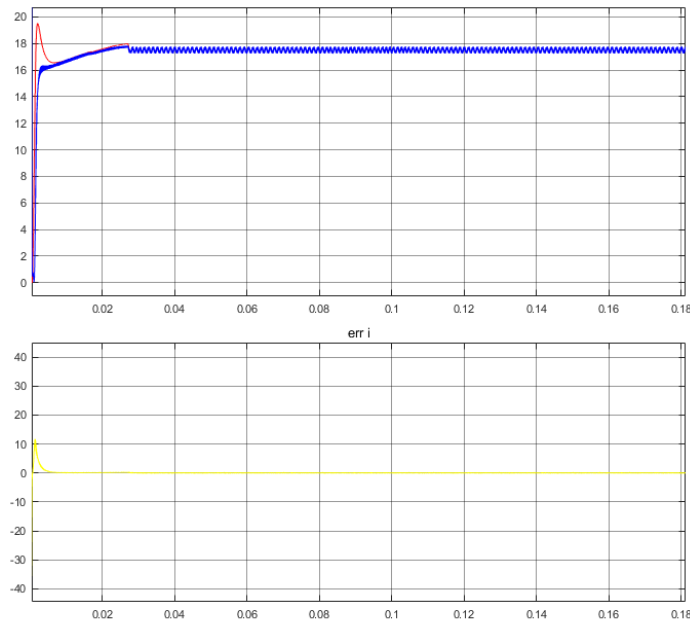


Fig. 4.25 Output/Reference current with error in Simulink using MPPT+Current Loop (180°C)

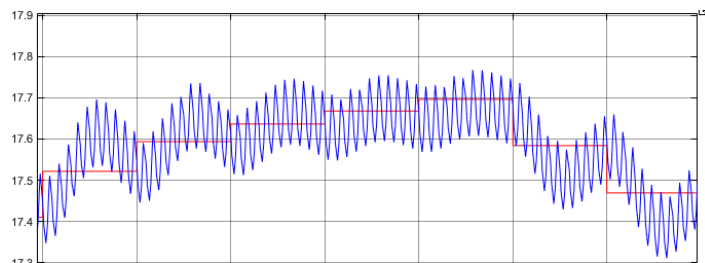


Fig. 4.26 Output/Reference current Zoom (180°C)

Fig. 4.25 represents the comparison between the reference current (red plot) realized by the MPPT and the output current (blue plot) which is supposed to follow the reference, and actually it can do it. in Fig. 4.26 the view is zoomed and it can be observed that the little red steps are followed by the output with light oscillations. The value of the output current should be approximately around 19 A, in the simulation it is a little lower than 18 A.

The prove that explains the right functioning of the MPPT is demonstrated in Fig. 4.27:

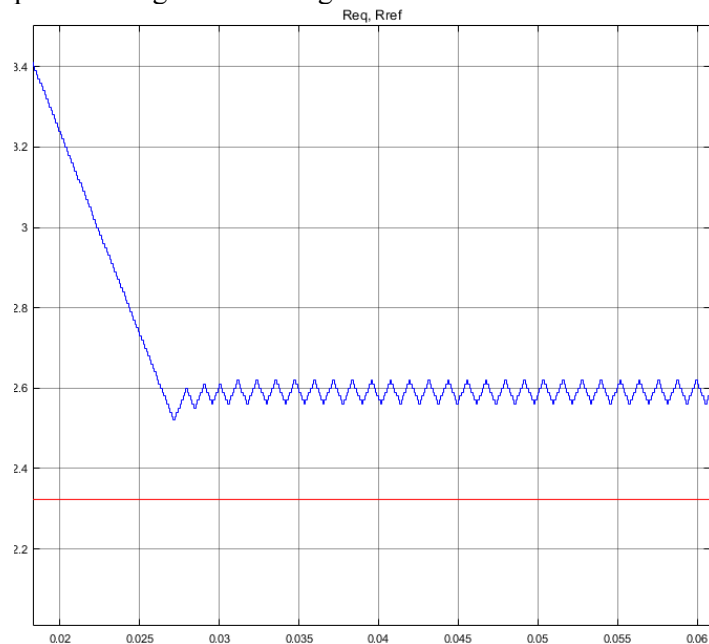


Fig. 4.27 Source and Load Resistances comparison (180°C)

The load resistance (in blue) is going down to the source resistance reference. It stops before, but it places in stability in a little range. The Buck duty cycle obtained from the control block is depicted in red in Fig. 4.28.

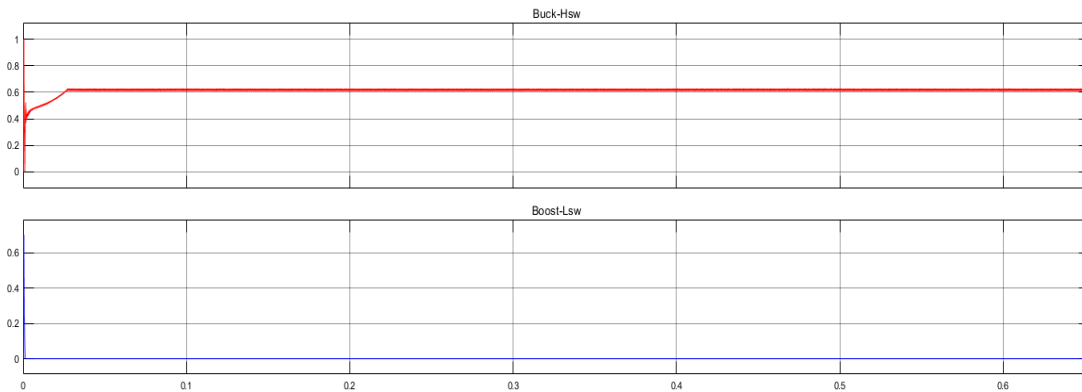


Fig. 4.28 Duty Cycles obtained at 180°C with MPPT+Current Loop

Also the Boost mode of the converter is tested and controlled, in fact next picture (Fig. 4.29) is related to the Simulink simulation at $\Delta T=50^{\circ}\text{C}$. From previous calculation, the output current should be 1.71 A, the simulation shows a similar behavior a little lower, focused in Fig. 4.30. In Fig. 4.31, instead, is illustrated the comparison of the source reference resistance (in red) to the load one (in blue), computed by the IC modified algorithm. Even though they are not the same, the result is quite satisfactory.

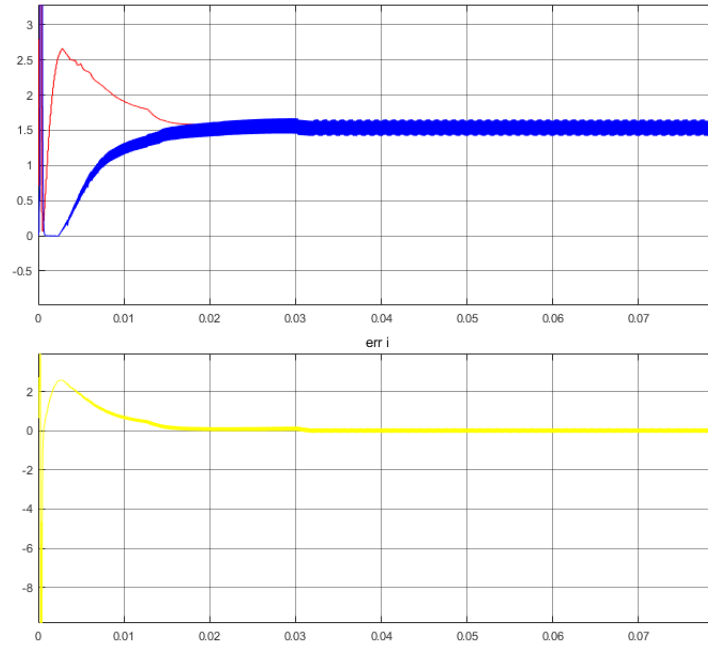


Fig. 4.29 Output/Reference current with error in Simulink using MPPT+Current Loop (50°C)

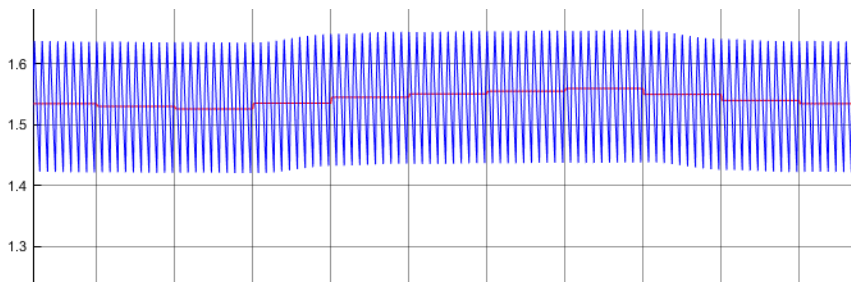


Fig. 4.30 Output/Reference current Zoom (50°C)

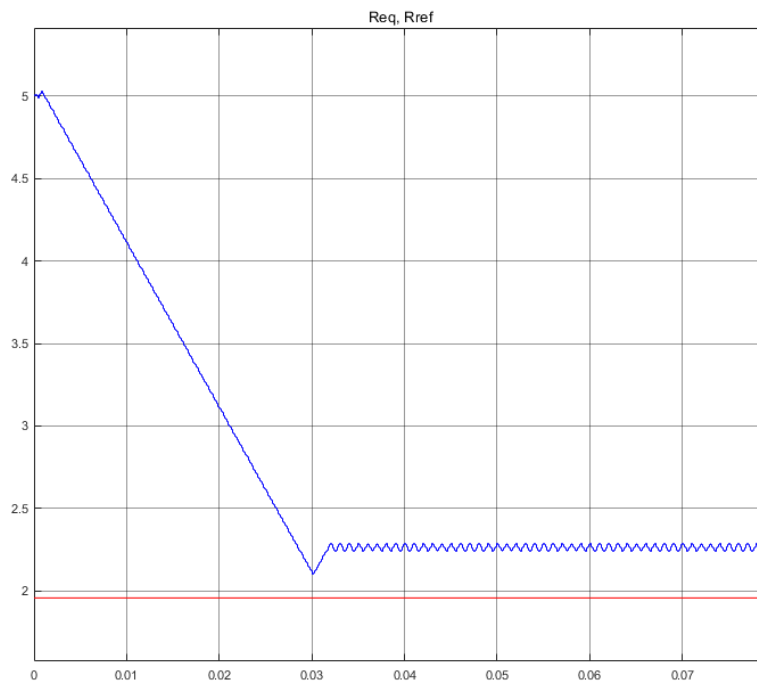


Fig. 4.31 Source and Load Resistances comparison (50°C)

Future developments, implementation and conclusions

FUTURE DEVELOPMENTS

The previous control strategies are based on the partition of the Non Inverting Buck-Boost converter in separated Buck and Boost. Thus only one duty cycle is obtained and it is referred to the relative operation mode of the DC-DC. One possible solution is the addition of a new block (Fig. 5.1), which inside (Fig. 5.2) there is a function capable to split one duty reference in two suitable values for SW1 and SW2.

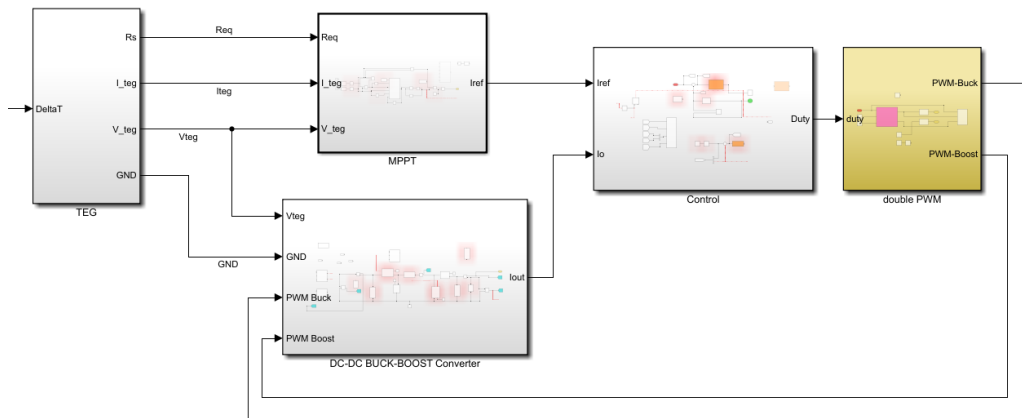


Fig. 5.1 New block addition in Simulink

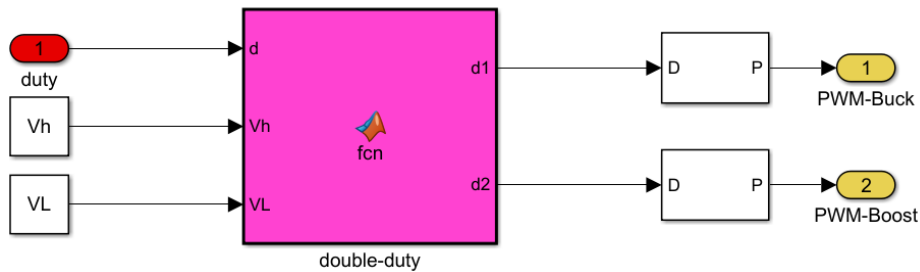


Fig. 5.2 Duty Cycle split Block Simulink

The principle lies in creating two different carriers to be compared to the duty cycle reference [17], from which two driving signals are achieved (Fig. 5.3):

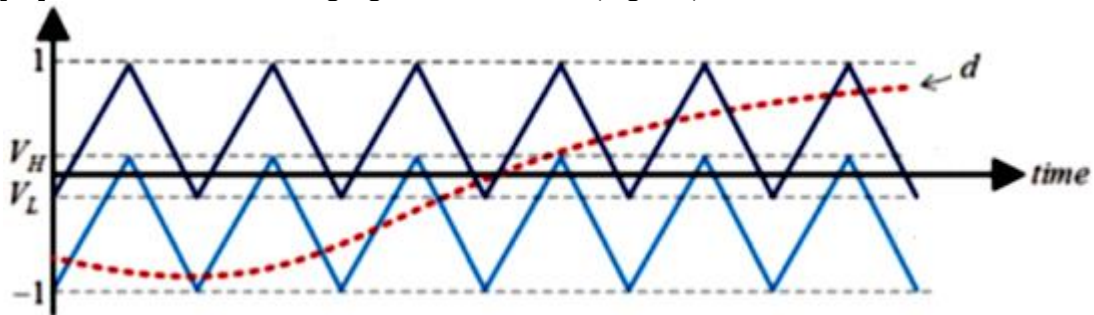


Fig. 5.3 Duty cycle compared to two carriers

Then the different operation mode (Table 15) is defined by the value of the reference d , which corresponds to the output of the control block and the input of the new one.

Operation Mode	Reference
Buck	$-1 < d < V_L$
Boost	$V_L < d < V_H$
Buck-Boost	$V_H < d < 1$

Table 15

And for specific conditions due to the carriers values, the duty cycle of each switch is obtained and shown in Table 16:

Duty Cycle	Condition	Result
Buck	$d < -1$	$d_{Buck} = 0$
	$-1 \leq d \leq V_H$	$d_{Buck} = \frac{1+d}{1+V_H}$
	$d > V_H$	$d_{Buck} = 1$
Boost	$d < V_L$	$d_{Boost} = 0$
	$V_L \leq d \leq 1$	$d_{Boost} = \frac{d-V_L}{1-V_L}$
	$d > 1$	$d_{Boost} = 1$

Table 16

IMPLEMENTATION

The prototypes realized in laboratory are four switch Non Inverting Buck-Boost converters (Fig. 5.4 and Fig. 5.5).

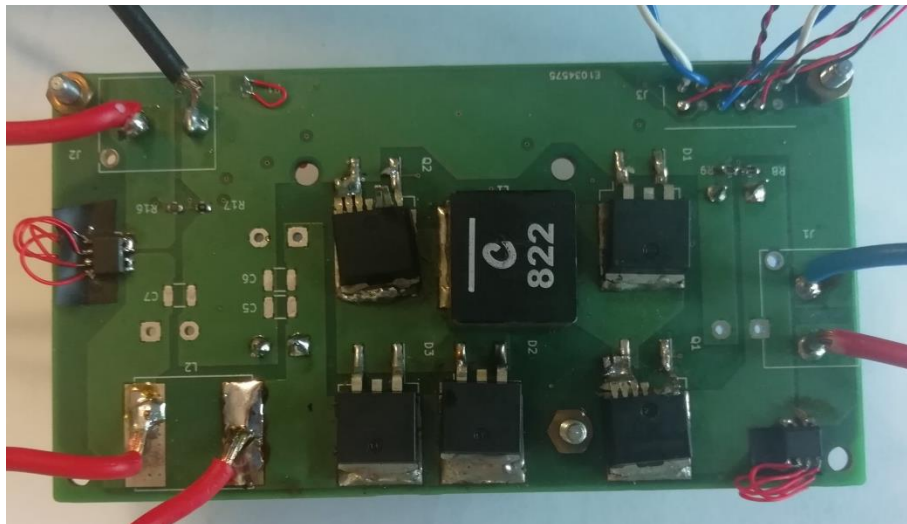


Fig. 5.4 First lab prototype

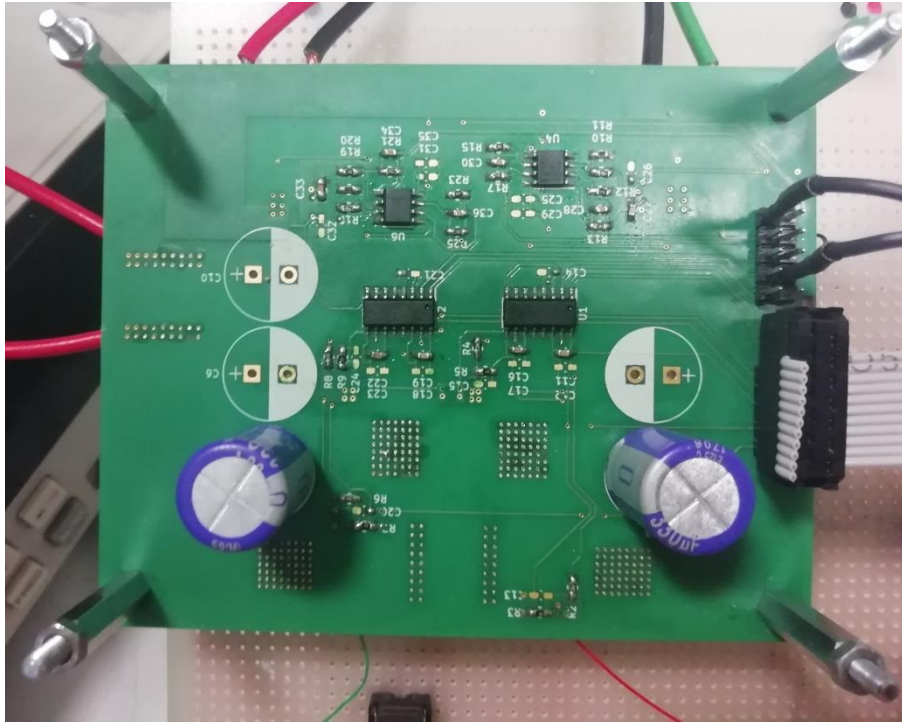


Fig. 5.5 Second lab prototype

The choice to adopt the synchronous rectification is made after some considerations about efficiency. In fact, as seen in previous chapters, the diode losses could be very significant in high current applications, they can completely damage the total efficiency of the converter. Replacing two MOSFETs instead of two diodes (basic scheme in Fig. 5.6) would lead to the reducing of conduction losses.

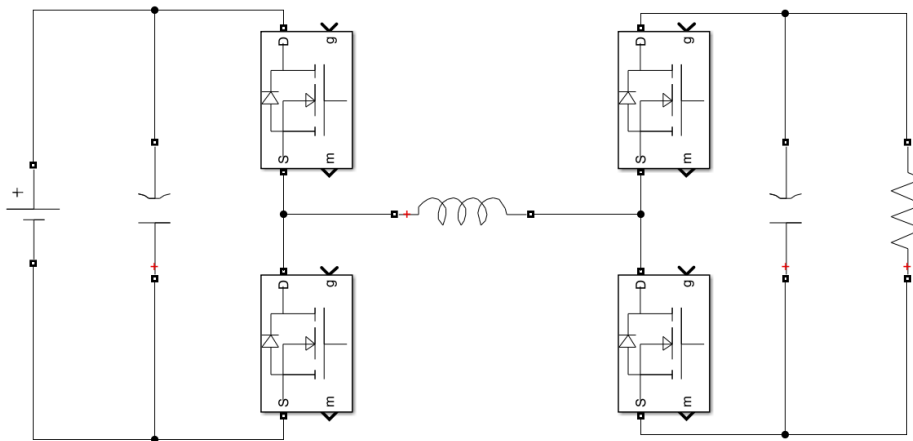


Fig. 5.6 4sw NIBB converter scheme

Because of at lower input voltage more conduction losses are generated, the result would be an efficiency improvement especially at small values of V_{in} .

The circuit, however, it is made of four switches. It means that in Buck-Boost mode each of the four components dissipates switching and conduction powers. Then as a result its efficiency is lowest in Buck-Boost operation mode. What is lost in this case is achieved with the reduction of the conduction losses caused by the diodes, then it is possible with the four switch Buck-Boost converter to reach higher levels of efficiency.

The prototypes have been tested, closing two of the possible switches, in order to calculate the power dissipated, hence the efficiency, of the Buck and of the Boost operation mode.

For every test:

- Specific voltage and current are applied to the input from a power supply;
- Duty cycle is adjusted for the purpose;
- Output voltage and current are measured from a resistive load;
- Input, output and dissipated power are calculated;
- Efficiency is obtained.

Table 17 and Table 18 show the measured values of both operation modes. Then the efficiency is represented as a function of the input voltage in Fig. 5.7 and it is compared to the efficiency calculated previously through the given dataset.

Boost Measured Values					
Vin [V]	Iin [A]	Pin [W]	Vout [V]	Iout [A]	Pout [W]
3.3	1.55	5.115	13.3	0.29	3.857
4.1	2.1	8.61	13.5	0.52	7.02
4.2	2.45	10.29	13.55	0.61	8.2655
5	2.8	14	13.7	0.86	11.782
5.6	2.95	16.52	13.5	1.07	14.445
6	3.38	20.28	13.5	1.34	18.09
6.5	3.35	21.775	13.35	1.47	19.6245
7	3.57	24.99	13.6	1.66	22.576
7.5	3.9	29.25	13.5	1.95	26.325
8	4.1	32.8	13.5	2.21	29.835
8.45	4.35	36.7575	13.3	2.5	33.25
9.1	4.38	39.858	13.5	2.63	35.5050
9.4	4.8	45.12	13.5	3	40.5
10	4.8	48	13.45	3.31	44.5195
10.5	5.15	54.075	13.5	3.7	49.95
11	5.45	59.95	13.55	4.15	56.2325
11.5	5.5	63.25	13.4	4.4	58.96

Table 17

Buck Measured Values					
Vin [V]	Iin [A]	Pin [W]	Vout [V]	Iout [A]	Pout [W]
14.65	4.5	65.925	11.02	5.2227	57.5547
14.99	4.8	71.952	11.79	5.5877	65.8787
15.73	6.5	102.245	12.26	7.4303	91.0955
16.73	6.8	113.764	12.92	7.8303	101.1675
17.67	6.5	114.855	12.98	7.8667	102.1093
18.95	7.4	140.23	12.88	9.6119	123.8018
19.78	7.1	140.438	12.89	9.6194	123.9941
20.8	8.6	178.88	12.82	11.8704	152.1781
21.77	8.2	178.514	12.83	11.8796	152.4156
22.73	9.9	225.027	12.57	15.1446	190.3673
24.74	9.7	239.978	12.73	15.3373	195.2445
24.74	9.5	235.03	12.84	15.4699	198.6333

Table 18

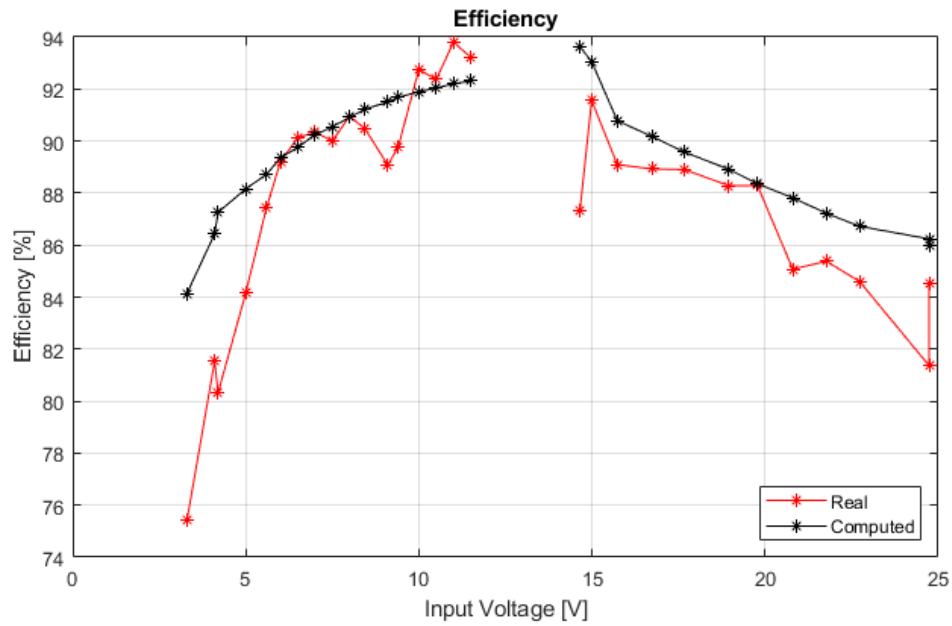


Fig. 4.7 Real and Computed Efficiency Comparison

CONCLUSION

The final proposed solution, consists in the Non Inverting Buck-Boost converter control by the usage of TI DSP control card (in Fig. 5.7).

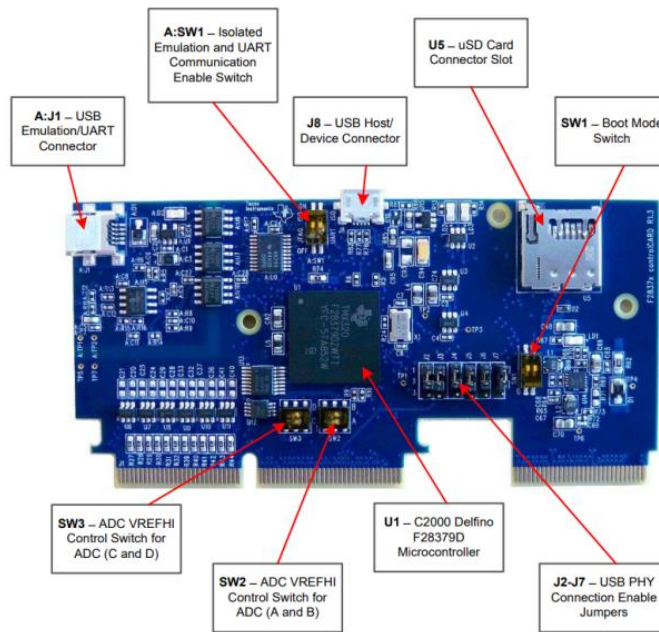


Fig. 5.7 DSP control card

Considering also the presence of the carrier board, which is populated with CAN transceivers (for communication), analog connections (i.e. temperature sensors) and signal conditioning circuits, the entire device could be imagined like in the Fig. 5.8.

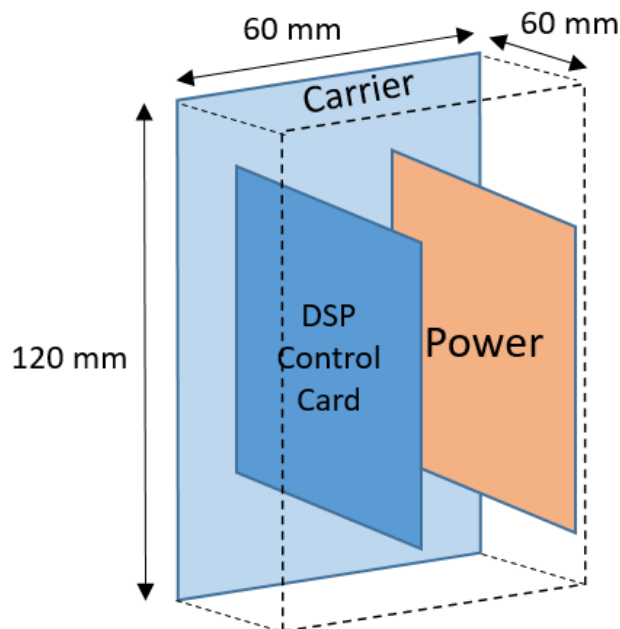


Fig. 5.8 Possible device sizes

References

- [1] www.sustainability.stackexchange.com/questions/1061/what-are-the-pros-and-cons-of-electric-motors-vs-internal-combustion-engines
- [2] Chuang Yu, K.T. Chau, “Thermoelectric automotive waste heat energy recovery using maximum power point tracking”, 2009
- [3] www.web.babblers.fr/document/show/automotive-exhaust-gas-recirculation-2018-industry-market-size-trends-growth
- [4] www.crossroadstoday.com/story/39477134/automotive-exhaust-gas-recirculation-system-market-2018-global-size-trends-share-industry-segments-regional-analysis-and-competitive-landscape
- [5] www.searchnetworking.techtarget.com/definition/Seebeck-effect
- [6] Lauri Kutt, Matti Lehtonen, “Automotive waste heat harvesting for electricity generation using thermoelectric Systems – an overview”, 2015
- [7] www.en.wikipedia.org/wiki/Thermoelectric_generator
- [8] Robin Vujanic, “Design and Control of a Buck-Boost DC-DC Power Converter”, 2008
- [9] Maddaleno Franco, Lacirignola, “Appunti Power Electronics”, 2015
- [10] www.circuitspecialists.com/blog/power-supplies-switch-mode-vs-linear
- [11] Molan Li, Shaohui Xu, Qiang Chen, Li-Rong Zheng, “Thermoelectric-Generator_based DC-DC Conversion Networks for Automotive Applications”, 2011
- [12] Vijay Choudhary, Timothy Hegarty, David Pace, “Under the hood of a noninverting buck-boost converter”, Texas Instrument, 2016/17
- [13] Alan Martin, Marc Davis-Marsh, Giuseppe Pinto, Ismail Jorio, “Capacitor selection for DC/DC converters: what you need to know to prevent early failures, and reduce switching noise”, 2012
- [14] Rhom semiconductors, “Efficiency of Buck Converter”, 2016
- [15] Fernando Lessa Tofoli, Denis de Castro Pereira, Wesley Josias de Paula, “Comparative Study of Maximum Power Point Tracking Techniques for Photovoltaic System”, 2015
- [16] Abraham Dandoussou, Martin Kamta, Laurent Bitjoka, Patrice Wira, Alexis Kuitche “Comparative study of the reliability of MPPT algorithms for the crystalline silicon photovoltaic modules in variable weather conditions”, 2016
- [17] Ilan Aharon, Doron Shmilovitz, Alon Kuperman “Robust output voltage control of multimode non-inverting DC-DC converter”, 2015